Journal of Marine Research, 69, 1–37, 2011

Journal of
MARINE RESEARCH

Volume 69, Number 1

Dispersion and connectivity estimates along the U.S. west coast from a realistic numerical model

by Patrick T. Drake[1,2], Christopher A. Edwards[1] and John A. Barth[3]

ABSTRACT

Near-surface particle dispersion, larval dispersal and connectivity along the U.S west coast were explored using a realistic numerical model of the California Current System. Seasonal model velocities were qualitatively and quantitatively evaluated using Global Drifter Program data. The model displayed a clear seasonal cycle of eddy energy near the coast with energy maxima southwest of major headlands. Eddy speeds were correlated with drifter-based estimates during summer and fall when compared spatially. Over six million passive, Lagrangian particles were released in the upper 20 m of the water column within 10 km of the California and Oregon coasts and tracked for 7 years. The effect of subgridscale vertical turbulence was parameterized with a random walk model. Resulting trajectories yielded climatological maps of particle dispersion. Particle densities varied with release region, release season and time-since-release. Dispersal distances and coastal connectivity varied with season of release, release location, release depth and pelagic larval duration (PLD). Connectivity was clearly influenced by major geographic features such as the Gulf of the Farallones and Cape Mendocino. Given a moderate (30–60 day) PLD, mean dispersal distances varied from ~10–230 km, with standard deviations of ~130–220 km. For release locations from Palos Verdes to Point Sur, the primary direction of dispersal was northward for a moderate PLD, regardless of season. For long PLDs (120–180 day), mean dispersal distances were larger (~40–440 km), with standard deviations of ~330–540 km. In winter given a long PLD, dispersal was primarily southward for release locations north of Point Arena. Increasing release depths to 40–60 m altered mean dispersal distances by 50–250 km polewards, but had little effect on standard deviations. Point Conception did not act as a barrier to dispersal for source regions in the Southern California Bight.

1. Ocean Sciences Department, University of California, Santa Cruz, California, 95064, U.S.A.
2. Corresponding author. ***email: pdrake@ucsc.edu***
3. College of Oceanic and Atmospheric Sciences, Oregon State University, Corvallis, Oregon, 97331, U.S.A.

1. Introduction

Dispersion associated with coastal circulation impacts many oceanographic problems of practical interest, such as the offshore flux of carbon from upwelling zones, transport of pollutants from nearshore sources, search and rescue operations, and appropriate design of marine reserves. Planktonic organisms drift with ocean currents and disperse due to the complexity of current shear and its temporal variability. Many nearshore and shelf species are relatively sedentary or sessile as adults but undergo an early planktonic larval stage. As a result, the maintenance of coastal communities and their alongshore distribution are influenced by circulation through the transport, dispersion and eventual return of planktonic larvae to habitable coastal sites. However, the degree of connectedness between populations is one of the major unanswered questions in marine ecology (Warner *et al.,* 2000). While marine connectivity is determined ultimately by both physical and biological factors (e.g., predation, behavior, available food resources, and habitat), understanding potential connectivity due to circulation alone is an important baseline analysis from which the impact of these effects can be determined. Such information can assist management decisions such as the effective design of marine reserves and protected areas (Botsford *et al.,* 2001; Kinlan and Gaines, 2003; Shanks *et al.,* 2003; Karlson, 2006).

Because dispersion results from differences in time-integrated transport following fluid parcels, it is often studied from a Lagrangian perspective. Off the U.S. west coast within the California Current System (CCS), there have been numerous observational studies of near-surface, Lagrangian dispersion (Davis, 1985; Poulain and Niiler, 1989; Brink *et al.,* 1991; Swenson and Niiler, 1996; Dever *et al.,* 1998; Brink *et al.,* 2000; Zhurbas and Oh, 2003). These experiments have successfully estimated mean current patterns, eddy kinetic energy, and diffusivities in the CCS using real oceanic drifters and have revealed interesting components of the circulation. However, as discussed by Mitarai *et al.* (2009), the sparse spatiotemporal coverage of real drifters limits their usefulness to quantify transport paths probabilistically. Source-destination relationships for particle trajectories are particularly difficult for observational studies to quantify.

The numerical simulation of drifter trajectories using currents from ocean circulation models represents an alternate approach toward studying ocean dispersion. Within the CCS, Lagrangian modeling studies have illustrated potentially important transport pathways (Cervantes and Allen, 2006; Pfeiffer-Herbert *et al.,* 2007; Carr *et al.,* 2008), and recent efforts using very large numbers of virtual drifters have begun to yield statistical descriptions of transport and connectivity within limited geographic portions of the California coast (Mitarai *et al.,* 2008; 2009; Drake and Edwards, 2009; Petersen *et al.,* 2010; Kim and Barth, 2011).

Despite these advances, a comprehensive statistical description of dispersion along the full U.S. west coast has not been achieved. The purpose of the present study is to investigate dispersion over much of this domain, calculating oceanic probability density functions for particles released from nearshore sites and quantifying the resulting connectivity between coastal regions when virtual drifters are parameterized to remain planktonic

for specified durations. We use a realistic numerical model of the CCS to drive particle transport, exploring the impact of coastal release location, depth range, and season. Rather than identify physical mechanisms responsible for particle paths, such as specific eddies, fronts or smaller-scale processes, we concentrate on net climatological probabilities. Statistics are determined from model runs over 7 years (2000–2006) with millions of passive particles released between Palos Verdes in southern California and Heceta Bank in Oregon. Connectivity is estimated for two competency time-windows, representing either moderate (30–60 day) or long (120–180 day) pelagic larval durations (PLDs). These PLDs represent the approximate planktonic periods of many inner and outer shelf species, respectively (Shanks and Eckert, 2005).

Within this paper, we follow the terminology of Pineda *et al.* (2007) and refer to larval transport as the net movement of larvae from one horizontal location to another. When the larvae are completely passive particles, this movement is synonymous with horizontal oceanic dispersion (Largier, 2003). This transport contributes to, but is distinct from, larval dispersal, which refers to the net movement from a spawning source location to a settlement site.

2. Model description

a. ROMS

Our implementation of the Regional Ocean Modeling System (ROMS, Song and Haidvogel, 1994; Shchepetkin and McWilliams, 2005) encompassed most of the U.S. portion of the CCS, ranging from northern Baja California to Washington State (−134° to −116.5°E and 30° to 48°N, Fig. 1). ROMS has been successfully used in the past to study the CCS on both regional and larger scales (Marchesiello *et al.,* 2003; Cervantes and Allen, 2006; Ivanov *et al.,* 2009; Veneziani *et al.,* 2009). Our model implementation is very similar to that described in Veneziani *et al.* (2009), except that the horizontal resolution is increased to 1/30 degree and ocean bathymetry is improved, based on a combination of the 2001 version of ETOPO2 (http://www.ngdc.noaa.gov/mgg/global/etopo2.html) and, where available, the National Geophysical Data Center 3-arcsecond Coastal Relief Model (http://www.ngdc.noaa.gov/mgg/coastal/coastal.html). The degree resolution used corresponds to an approximate grid spacing of 3.7 km meridionally and 2.5–3.2 km in the zonal direction. The model contained 42 terrain-following vertical levels in an s-coordinate scheme, with the vertical resolution varying both vertically and horizontally. Typical, near-surface resolution was roughly ~0.3–4 m over the shelf and slope and ~8–20 m over the deep ocean. Topographic smoothing ensured that the ratio of the change in ocean depth between adjacent grid points to the local depth ($|\delta h|/h$) was less than 0.25.

As in Veneziani *et al.* (2009), surface forcing was provided by daily-averaged fields from the Coupled Atmospheric Mesoscale Prediction System (COAMPS™) (Hodur, 1997; Hodur *et al.,* 2002). This system consists of four nested grids centered around Monterey Bay, resulting in relatively high resolution along the California and Oregon coasts

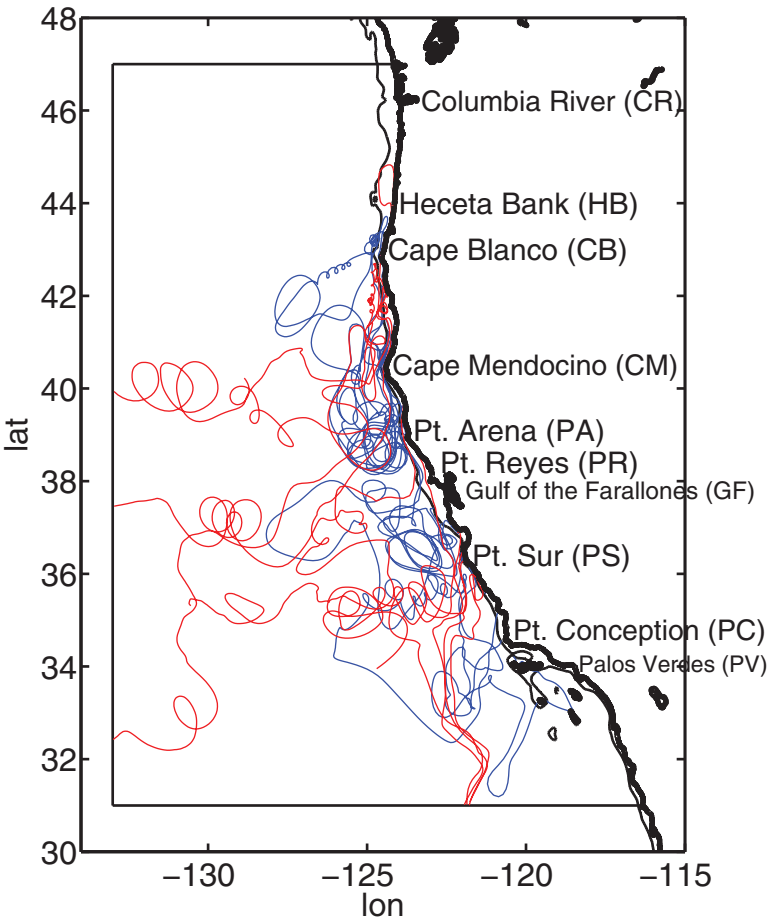

Figure 1. Model domain showing major promontories. Inner rectangle shows the boundaries used for all statistics. Blue trajectories are the paths of 10 randomly selected particles released in April of 2000, that eventually settled during a 120–180 d PLD. Red trajectories show 10 randomly selected particles from the same release that did not settle during this PLD. Fine black line shows the 250-m isobath in the model bathymetry.

(3–9 km). Riverine outflow and tidal motion were excluded from the implementations, as was San Francisco Bay and all other estuaries. Lateral boundary conditions were provided from monthly climatology given by the National Oceanographic Data Center World Ocean Atlas (WOA05) (Antonov *et al.,* 2006; Locarnini *et al.,* 2006; Collier and Durack, 2006). Radiation conditions and a sponge layer were applied at and near the boundaries to match the ROMS solution to the exterior fields.

Subgridscale vertical mixing was accomplished with the Generic Length Scale (GLS) (Umlauf and Burchard, 2003) turbulence closure scheme, using k-ω parameters (e.g.,

Warner *et al.,* 2005). In addition, we added random vertical motion to the particle velocities. This particle mixing was performed offline and had no effect on Eulerian fields. The model was spun up for seven years with an initial state given by the WOA05 climatology and geostrophic velocities referenced to 500 m. Experiments revealed that overall results of this study were relatively insensitive to changes in the lateral boundary conditions or vertical mixing scheme.

Computational cost limited the model horizontal resolution to 2.5–3.7 km, which is greater than the offshore extent of the inner shelf in many areas of the U.S. west coast. The model also did not contain many physical processes important to the circulation in relatively shallow depths ($\leq$30 m), such as barotropic and internal tides, the sea breeze and fresh-water input. The circulation in this nearshore zone is not well resolved, and particle densities presented below represent mostly the effects of larger-scale processes acting over the mid-shelf, slope and deeper water.

b. Lagrangian particles

i. Releases and settling. Model floats were seeded from Palos Verdes to Heceta Bank (33.7–44.0°) on ROMS horizontal grid points (for density) between 1 and 10 km of the functional model coastline, excluding San Francisco Bay, other estuaries and all islands (Fig. 1). The 10-km offshore extent corresponds very roughly to a water depth of ~250 m along most of the coastline, notable exceptions being wide-shelf regions such as the Gulf of the Farallones and Heceta Bank. The functional coastline was defined as the location of no normal flow along the continuous mainland. This coastline was then subdivided into 70 individual potential source and settling locations, or cells, each with an approximately 400 km^2 area and 10 km offshore limit (Fig. 2). The discrete nature of the coastline resulted in small variability in the precise cell area with a coefficient of variation ~0.03. Equal cell area ensures as a null hypothesis that equal settlement would occur given a random distribution of settling particles.

At each horizontal grid point (for density), 8 floats were given an initial uniform random vertical distribution from the surface to a depth of 80 m or the ocean bottom, whichever was shallower. To investigate dispersal by release depth range (e.g., 0–20 m, 40–60 m), we sub-sampled floats by release depth. Unless stated otherwise, all results presented refer to our default case of 0–20 m. Statistics were not sensitive to depth changes within this near-surface zone, likely due to the vertical random walk employed (described below). However, choosing an alternate release range of 40–60 m did produce important differences to dispersal and connectivity (see coastal connectivity, below). The number of floats released per cell within 0–20 m differed due to the irregularity of the coastline and alongshore variations in water depth (mean 1,800 month^{-1}, standard deviation 650 month^{-1}). In statistics involving the full seeded coastline (FSC), floats were also sub-sampled to give equal weight to each release cell. Floats were released every other day from the same (x, y, z) locations for seven years, from January 1, 2000 to December 30, 2006, and over 6 million floats were analyzed. With this seeding and sampling, the

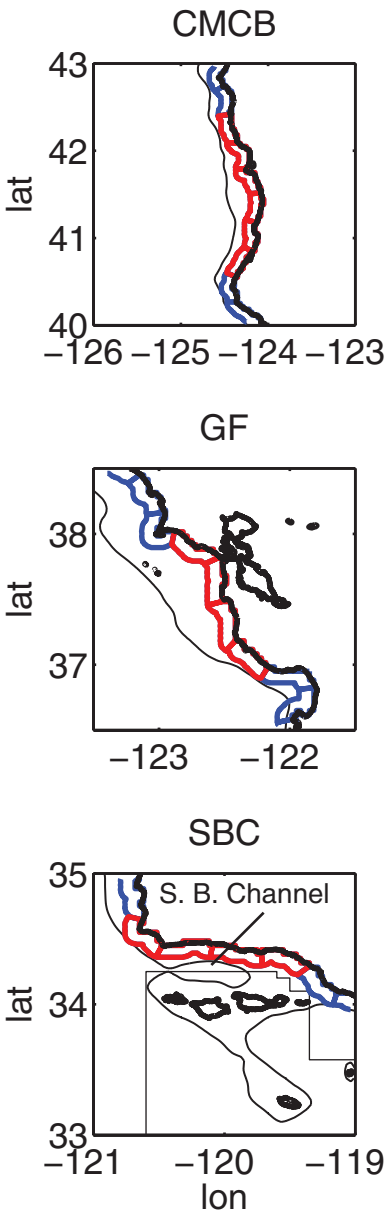

Figure 2. Particle release cells in and surrounding the three major release regions used to calculate the two-dimensional PDFs (see Figs. 6, 7 and 8). Red coloring delineates each PDF region. Fine curved line is the 250-m isobath. Bottom panel shows the Southern California Bight and polygon used to excluded settlement to the Channel Islands.

seasonal, climatological connectivity matrices presented below are based on ~38,000 individual trajectories released per cell. (The number that ultimately settled was considerably smaller.) Sensitivity studies (not shown) using only a small fraction (~15–20%) of the total number of trajectories, chosen at random, revealed that results were not sensitive to the total number of floats employed. However, changes to release region, depth and time were important. In addition to the individual cells, three larger-scale source regions were identified for study (Fig. 2), representing releases from three distinct regions of the CCS (Checkley and Barth, 2009). The northern region sits in the embayment formed by the Cape Mendocino and Cape Blanco headlands (CMCB region). The central region lies between Monterey Bay and Point Reyes and is most representative of the Gulf of the Farallones (GF region). The southern region lies along the mainland side of the Santa Barbara Channel (SBC region).

To quantify connectivity, settlement occurred if a particle was found within a coastal release cell (bounded by a 10-km offshore limit) during the competency window of its PLD, either 30–60 or 120–180 days-since-release. Because settlement in nature is more dependent on bottom topographic depth than on linear distance from shore, an alternate settlement criteria using the 250-m isobath was also investigated. A particle could settle only once for a given PLD. Exact settling locations ranged over the entire shelf, but settlement was typically highest within a few kilometers of the seaward edge of the cell or 250 m isobath.

Given the ~3 km grid spacing, the Channel Islands (Fig. 2, bottom panel) were not well resolved by the model. In this study we concentrate on the larger-scale, along-coast connectivity and exclude the Channel Islands as possible settlement locations. Settlement to the islands was prevented by forbidding settlement within the polygon shown in Figure 2, bottom panel. Smaller-scale connectivity in and around the Channel Islands and the Southern California Bight was extensively and well investigated by Mitarai *et al.* (2009).

ii. Trajectories. Simulated particle trajectories were calculated using an offline version of ROMS' internal drifter module. Floats were transported by the three-dimensional currents of the model and treated as purely passive, Lagrangian particles: $d\mathbf{x}_p/dt = \mathbf{u}(\mathbf{x}_p)$, where $\mathbf{x}_p$ is the three-dimensional particle position and $\mathbf{u}$ is the three-dimensional Eulerian model velocity at $\mathbf{x}_p$. The module interpolates the Eulerian model velocity linearly in all three spatial dimensions onto the particle positions. Positions are then integrated in time using a fourth-order Milne time-stepping scheme and fourth-order Hamming corrector step. Positions were calculated in model grid coordinates and later interpolated onto a Cartesian representation of the grid (x, y). Our offline version of the module utilized daily averaged currents, linearly interpolated to hourly values to match the hourly time-step of the floats. Experiments showed that increasing the temporal resolution of the currents to 12 hours, or decreasing the float time-step to 6 minutes had almost negligible effect on ensemble statistics, including the connectivity matrices. (Individual trajectories, however, quickly diverged given slight changes to the resolution and time step.)

A random vertical walk was added to the trajectories, simulating subgridscale particle mixing. We followed the procedure of Hunter *et al.* (1993), which accounts for random particle motion associated with a linearly varying diffusivity. As discussed by Ross and Sharples (2004), it is important that the random spatial kick given to any particle be small compared to the scale over which the vertical gradient of diffusivity changes appreciably. Otherwise, unphysical accumulation of particles in regions of low diffusivity may result (e.g., just below the mixed layer or just above the bottom boundary layer). Such accumulations were avoided using an adaptive time step for random vertical motion only. The step size, δt, was determined such that each particle's random adjustment be smaller than 1/8 of the minimum ROMS layer thickness at the particle's horizontal location. This procedure often resulted in time steps of a few seconds or less. The high computational costs of this traditional approach to a random walk suggests that innovative, lower-cost approaches to particle mixing are needed in the future, especially for large-scale, climatological studies employing million of particles.

To avoid potential impact of spurious model boundary effects, trajectories were truncated if and when they came within 1.0° of the domain's open boundaries (shown by the fine lines in Fig. 1). Each float was tracked for 180 days or until it encountered the edge of this inner domain. Float positions were recorded every 12 hours. All simulated particle statistics are derived from these 12-hourly instantaneous positions.

iii. Particle PDFs. The time axes of particle trajectories were converted from calendar time to days-since-release with a simple resorting. Histograms of particle locations were then calculated at different values of time-since-release using 100 km^2 bins. Histograms were converted to probability density functions (PDFs) by normalizing such that their integral over all space was unity at the time of release. This procedure was followed for each release cell and release month. PDFs were combined linearly in space and time to form climatological probability maps for seasons and regions, with final PDFs weighted per float. Seasonal PDFs from the SBC, GF and CMCB regions comprised 4–6 cells and over 130,000, 220,000 and 340,000 individual trajectories, respectively.

3. Model evaluation

a. Data and methods

We evaluate the model by comparing near-surface seasonal mean currents and eddy speeds to those of real surface drifters in the North Pacific Ocean. A processed and interpolated data set of both drifter position and velocity (Hansen and Poulain, 1996) was obtained from the Global Drifter Program (GDP), available electronically at www.aoml.noaa.gov/phod/dac/dacdata.html. Spatial maps of mean velocity can be constructed from Lagrangian drifter trajectories by binning in time and space, creating pseudo-Eulerian fields. This process can lead to errors and biases that result from either low sampling resolution or correlations between the true Eulerian velocity and particle concentrations

(Garraffo *et al.,* 2001; Davis, 1991). We do not attempt to calculate these biases here, but previous studies have shown that using GDP drifters will overestimate eddy energy for the CCS (Centurioni *et al.,* 2008), discussed below. Despite this error, the GDP drifters offer the best available estimate of the full velocity field, including the Ekman portion, which is critical for cross-shore transport and dispersal.

Because the data spatial coverage over the time-period of the model experiments (2000–2006) was insufficient to allow for a meaningful model-data comparison, we used the entire temporal extent of the GDP data set (1979–2009) to form climatological fields, using drogued drifters only. Velocity data were averaged annually and within seasons (winter: January–March; spring: April–June; summer: July–September; and fall: October–December), using $0.5° \times 0.5°$ spatial bins, a common approach for Lagrangian data (Veneziani *et al.,* 2004; Centurioni *et al.,* 2008). Data were not pre-averaged in time. The spatial bins covered the entire inner domain. Following Veneziani *et al.* (2009), bins with fewer than 5 independent measurements were not considered in the statistics. The number of independent measurement was calculated as $n\Delta t/T_L$, where n is the number of observations, Δt is the sampling interval in the GDP dataset (6 hours) and T_L is the Lagrangian decorrelation time scale for the near-surface California Current (2–7 days, Swenson and Niiler (1996)), and we used the lower bound of 2 days to preserve as much data as possible.

In general, agreement between model and data was best using surface Eulerian fields. However, because the real drifters were drogued to a nominal depth of 15 m, we interpolated the model Eulerian velocity to this depth for all statistics presented. Eulerian velocities were then averaged, using the same time and space bins as the data. The mean eddy speed, or the r.m.s. of the fluctuation velocity, $|\mathbf{u}'|_{\text{rms}}$, was then calculated from the mean fields. The fluctuation velocity was defined as, $\mathbf{u}' = \mathbf{u}(x, y, t) - \mathbf{U}(x', y')$, where $\mathbf{u}$ is the instantaneous two-dimensional vector velocity and $\mathbf{U}$ is its average over both time and space on the $0.5° \times 0.5°$ grid given by (x', y'). (Mean fields were not interpolated spatially when calculating fluctuation velocities.) Mean eddy speed is related to eddy kinetic energy, EKE, by $|\mathbf{u}'|_{\text{rms}} = \sqrt{2\text{EKE}}$, where $\text{EKE} = 0.5(u'^2 + v'^2)$, and u' and v' are the fluctuation eastward and northward velocities, respectively.

b. Mean flow

Modeled Eulerian and measured Lagrangian velocities were not well correlated over the model domain when compared spatially on a point-to-point basis as scalar components (using the $0.5° \times 0.5°$ grid). This occurrence is common in modeling studies, where real circulation features are often present in the model but displaced slightly in space and time due to both modeling errors and the nondeterministic nature of the dynamics (Centurioni *et al.,* 2008). Although poor spatial coverage in the GDP data set near the coast somewhat limits comparison, the seasonal mean flows in both the data and model have qualitatively similar spatial patterns, as shown by Figures 3 and 4. We color-code velocity vectors based on compass quadrant to help reveal directional patterns. Also, we have neglected to display

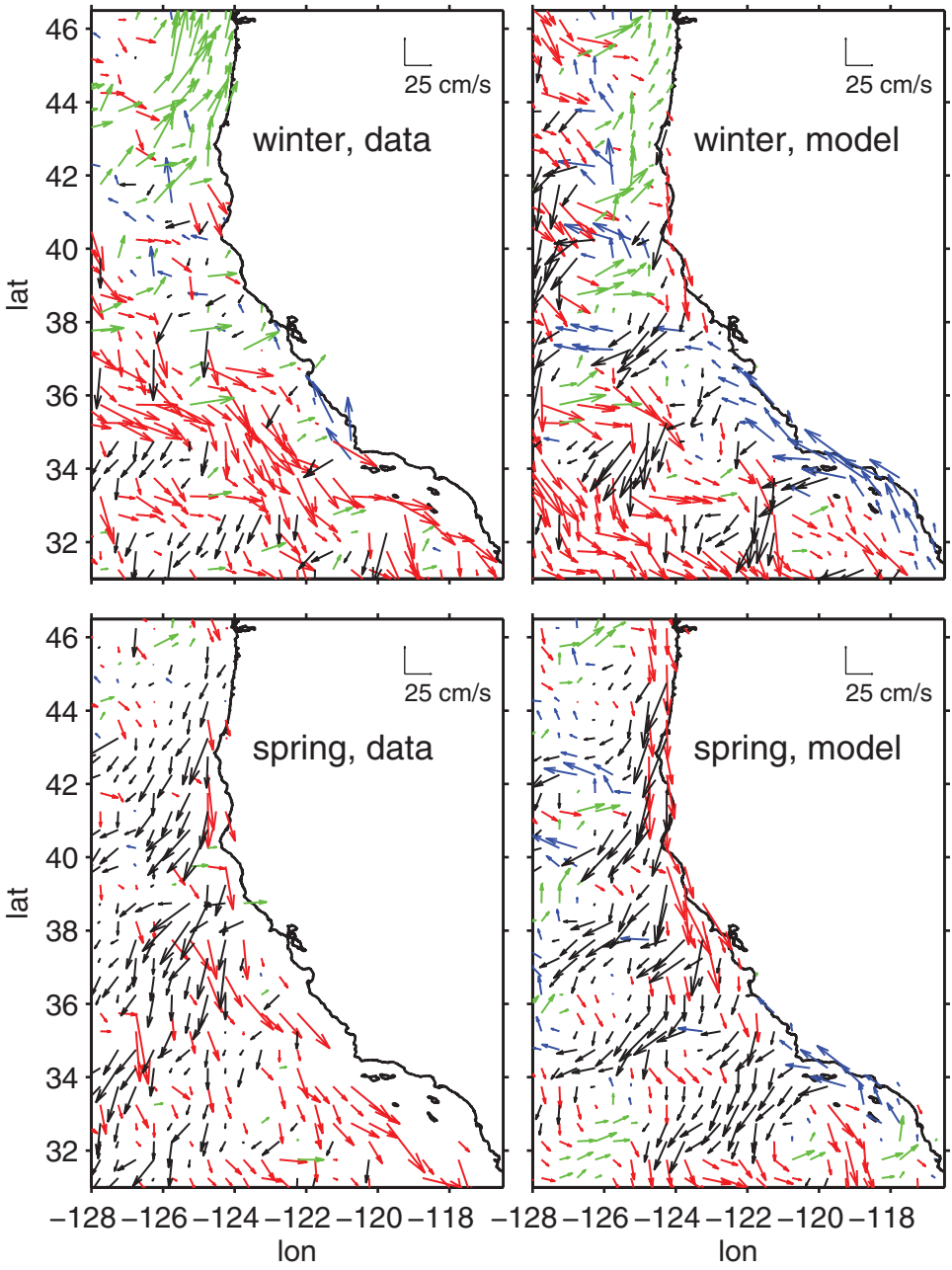

Figure 3. Season mean flow from the data (left column) and model (right column) for winter (top) and spring (bottom) when averaged in 0.5° × 0.5° bins. The data panels show a psuedo-Eulerian statistic calculated from real surface drifters drogued to 15-m depth from the GDP dataset. The model panels show the Eulerian velocity field at 15 m. Note the lack of data coverage near the coast in spring. Vectors are color-coded by compass quadrant to help reveal common circulation features: green, NE; blue, NW; black, SW; and red, SE.

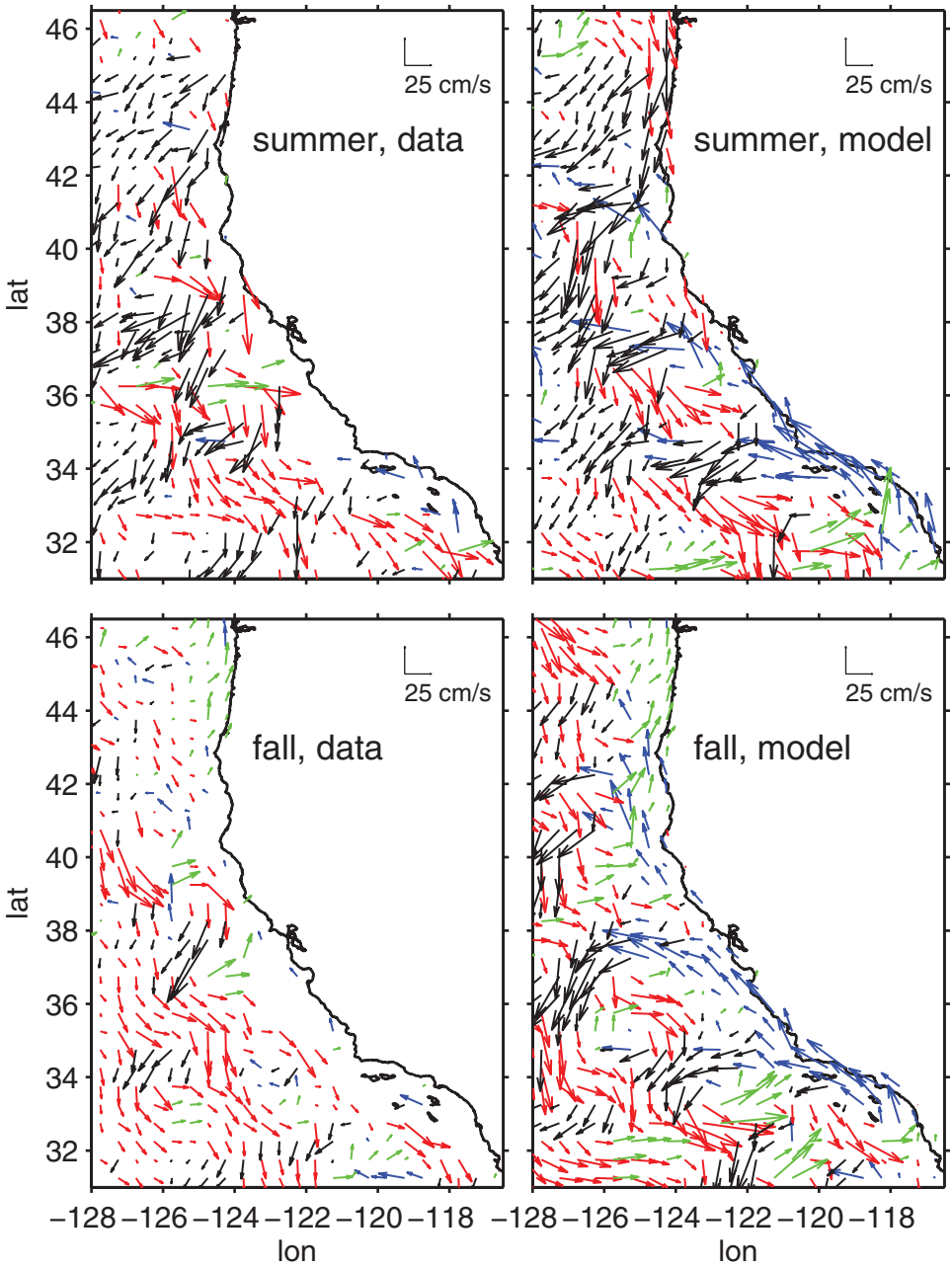

Figure 4. Season mean flow from the data (left column) and model (right column) for summer (top) and fall (bottom) when averaged in 0.5° × 0.5° bins. The data panels show a psuedo-Eulerian statistic calculated from real surface drifters drogued to 15-m depth from the GDP dataset. The model panels show the Eulerian velocity field at 15 m. Note the lack of data coverage near the coast in summer. Vectors are color-coded by compass quadrant to help reveal common circulation features: green, NE; blue, NW; black, SW; and red, SE.

the western portion of the domain for viewing clarity, but all statistics derive from the full inner domain shown in Figure 1.

Common wintertime features include: a semi-continuous poleward inshore coastal current (sometimes called the Davidson Current (Lynn and Simpson, 1987; Collins *et al.,* 2000)) extending from the Southern California Bight (model) or Point Conception (data) north to the Gulf of the Farallones (model) or Point Arena (data); near-shore poleward flow from Cape Blanco to the Columbia River; and a general pattern of southeastward transport further offshore, interspersed with pockets of southwestward flow.

In spring, both the model and data show equatorward nearshore flow north of Point Arena. In the northern portion of the domain, there is also a common pattern of southwestward flow further offshore becoming more southeastward near the southern boundary. The Southern California Eddy (Dong *et al.,* 2009) is well developed in the model at this time. However, drifter coverage is too sparse to discern its landward portion in the data. A wide offshore jet that is produced in the model at Point Conception in spring is absent in the GDP data.

In summer, a general pattern of southwestward flow offshore interspersed with pockets of southeastward transport is present in both the model and data. This pattern in spring and summer in both model and data differs from traditional seasonal maps of the California Current (CC) (Lynn and Simpson, 1987; Strub and James, 2000), which show the flow as much more uniformly southeastward and alongshore near the coast. This difference results from our presentation of the full velocity field, including the Ekman portion, as opposed to geostrophic velocity only, as calculated from altimetry or thermal wind.

In fall, a semi-continuous poleward inshore coastal current extending from the Palos Verdes to the Columbia River mouth can be seen in the model. The data shares this feature north of Cape Blanco, but due to the poor spatial coverage, the data reveals only part of this feature along central California. Common to both model and data is a general pattern of southeastward flow further offshore, interspersed with pockets of southwestward motion.

The counter-current has important consequences for the dispersion from the SBC region. Although the GDP data were sparse over the shelf and slope in spring and summer, the seasonal timing of the appearance of an inshore counter-current between Point Conception and Point Sur in the model agrees roughly with historical California Cooperative Oceanic Fisheries Investigations (CalCOFI) data (Lynn and Simpson, 1987, their Fig. 5): the current is clearly present in the model during fall and winter and primarily absent in spring and summer. Modeled poleward near-surface transport immediately at the coast in spring and summer in this region is limited to the shelf, inshore of the 250 m isobath, consistent with previous mooring measurements from the area (Chelton *et al.,* 1988).

c. Eddy speed

The eddy speed can be just as important to particle dispersion as the mean flow because it is fluctuation velocities that produce particle diffusion when viewing dispersion within a classic advection-diffusion paradigm (Swenson and Niiler, 1996). Diffusive transport can

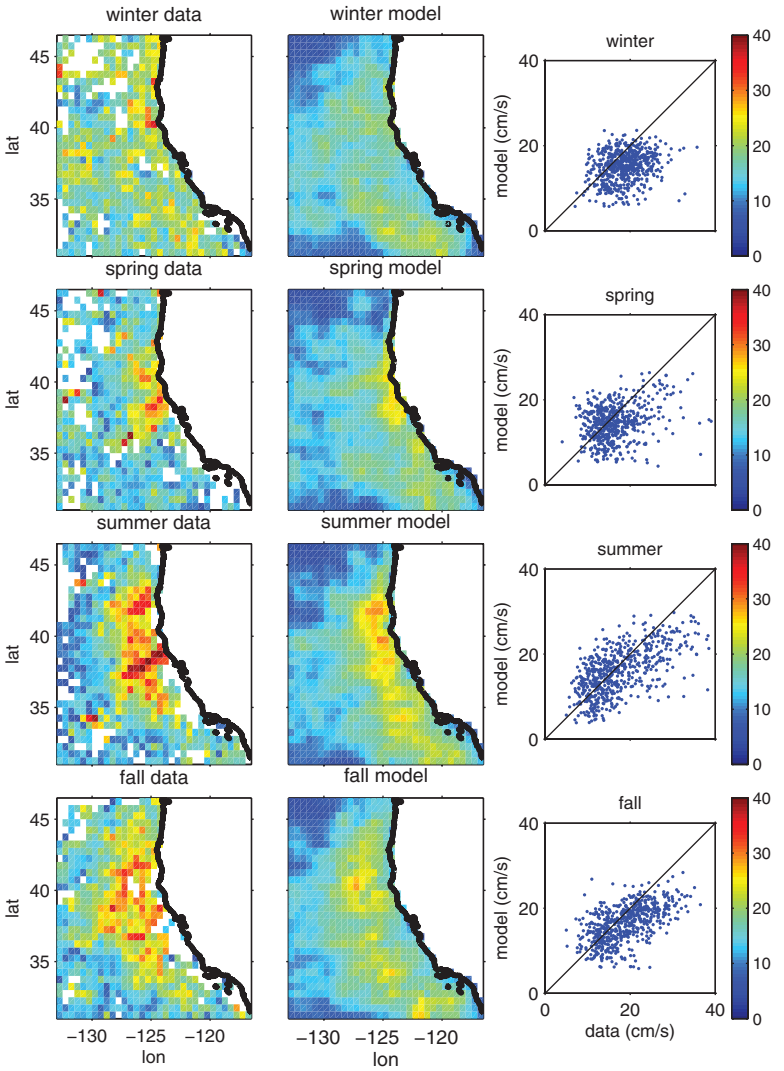

Figure 5. Seasonal eddy speed ($\sqrt{2}$EKE), from the GDP data set, left column, and the model, center column, when averaged over 0.5° × 0.5° spatial bins, from winter (top) through fall (bottom). Right column is a scatter plot of the data (x) verses the model (y). Color-scale units are cm s^{-1}. The data is a psuedo-Eulerian statistic from surface drifters drogued to 15-m depth, while the model panels show the Eulerian field at 15-m depth.

be greater than advective transport over relatively long time scales or averaging periods that capture current reversals (Largier, 2003), especially in the cross-shore direction near the coast where mean flows are relatively small (Ivanov *et al.,* 2008; Drake and Edwards, 2009). The CCS exhibits a seasonal cycle of eddy energy development (Kelly *et al.,* 1998;

Table 1. Eddy speed ($\sqrt{2}$EKE) statistics at 15 m depth using 0.5° × 0.5° spatial bins over the inner domain. The mean and std are in cm s^{-1}. *r* is the spatial correlation coefficient.

	Winter	Spring	Summer	Fall	Annual
Mean $\sqrt{2}$EKE					
Real drifters	18.6	16.4	17.4	18.7	19.0
model Eulerian	14.6	14.2	15.5	16.0	15.6
std $\sqrt{2}$EKE					
Real drifters	4.3	5.2	7.2	5.9	4.6
model Eulerian	3.8	4.4	5.4	4.6	4.2
r $\sqrt{2}$EKE					
Real drifters vs model Eulerian	0.24	0.29	0.61	0.55	0.52

Strub and James, 2000; Marchesiello *et al.,* 2003). Near-shore energy is a minimum in early spring when the onset of consistently upwelling-favorable winds establishes a strong upwelling front at the coast with an associated alongshore jet. The upwelling front devolves into a series of eddies, filaments and meanders over the spring and summer, with energy peaking in late summer or early fall and slowly propagating offshore.

The seasonal cycle is clearly present in the eastern portion of the domain in both the drifter data and model (Fig. 5). The cycle is also apparent, though at much reduced amplitude, when comparing mean eddy speed values over the entire inner domain (Table 1). Energy is highest in both the data and model immediately southwest of the large promontories in northern California, specifically Cape Blanco, Cape Mendocino and Point Arena. The model consistently underestimates the mean eddy speed and its spatial standard deviation by ∼10–20 percent. Point-to-point spatial correlations of the eddy speed are highest in summer and fall when the eddy field is most developed and localized near the coast. The number of statistically independent observations, N^*, available over the inner domain can be estimated from the spatial decorrelation scale. Choosing a decorrelation scale from Figure 5 of ∼3° for the largest features (consistent with the wavelengths reported by Strub and James (2000) of ∼300 km for the meandering coastal jet) yields $N^* \sim 20$. Using this value, only the summer, fall and annual correlations are significant to the 95 percent confidence level.

The discrepancy between eddy speeds displayed by the model and data may result from several factors. Biases in forcing fields, model errors (e.g., in subgridscale mixing), or model resolution can influence modeled eddy kinetic energy. In addition, the relatively short duration of the model (2000–2006) excludes some temporal variability captured by the longer GDP data set (1979–2009). However, the GDP eddy speed is likely an overestimate, as noted above. Many CSS drifters were deliberately launched into energetic eddies and filaments that retained the drifters for long periods, potentially biasing the measured energy high (Brink *et al.,* 1991; Kelly *et al.,* 1998; Centurioni *et al.,* 2008). Using

a statistical combination of both drifter and satellite sea level data, Centurioni *et al.* (2008) find that drifters alone overestimate the annual unbiased geostrophic eddy speed by ~20% (judging from their Fig. 6). This difference in energy is similar to the discrepancy we find here, suggesting that the true bias in our model may not be as large as implied by Figure 5 and Table 1. Ultimately, any eddy speed bias will result in systematically biased modeled standard deviations of dispersal distance. We expect that greater (lower) eddy energy would diffuse particles farther (less far) from their source locations and reduce (increase) settlement strength. A reader should be aware of this effect and consider our calculated dispersal distances as possibly biased low.

4. Climatological PDFs of dispersion

Seasonal, climatological particle densities from the SBC, GF and CMCB regions are shown in Figures 6, 7 and 8, respectively, at various snapshots in time-since-release for a shallow (0–20 m) release. Although we identify the PDFs by their season of release, PDFs at 120 days-since-release show the particle densities well into the following season. As they were normalized at time-of-release, changes in color indicate both diffusion within and float loss from the domain. After release, particles rapidly left their release depths and spread over the top 120 m of the water column, but most remained relatively shallow, with more than half found above 60 m, regardless of time, season or release depth. In general, the majority of floats remained within the inner domain during all seasons and investigation times (Table 2), although substantial float loss did occur from the SBC region due to the predominantly southward-flowing CC and the region's proximity to the southern boundary. Approximately half of the particles from this region in winter and spring were lost from the inner domain at 120 days-since-release, the start of the settling competency window for many species.

In our model, the SBC region exhibits poleward alongshore coastal transport during all seasons (Fig. 6). At 120 days-since-release, substantial float densities reach Point Arena for summer and fall releases and floats are found as far north as Cape Mendocino for the fall case. The northward transport is primarily a result of the inshore counter-current and northward flow found over the shelf, although these flows may be indistinguishable from the California Undercurrent during certain times of the year (Lynn and Simpson, 1987; Pierce *et al.,* 2000). In fall and winter, the counter-current ranges from the southern portion of the Southern California Bight to Monterey Bay and Gulf of the Farallones in the model (Fig. 3, top right panel; Fig. 4, bottom right panel). Data show the current also rounds Point Conception most times of the year at subsurface but relatively shallow depths (45 m) (Winant *et al.,* 2003).

In our results, the counter-current bifurcates near Point Conception, where one branch separates from the coast and becomes the southward-flowing arm of the Southern California Eddy and another limb continues poleward. This general pattern is consistent with mooring results which show a surface convergence at the point during most times of the year (Winant *et al.,* 2003), although the exact location of the convergence in the model

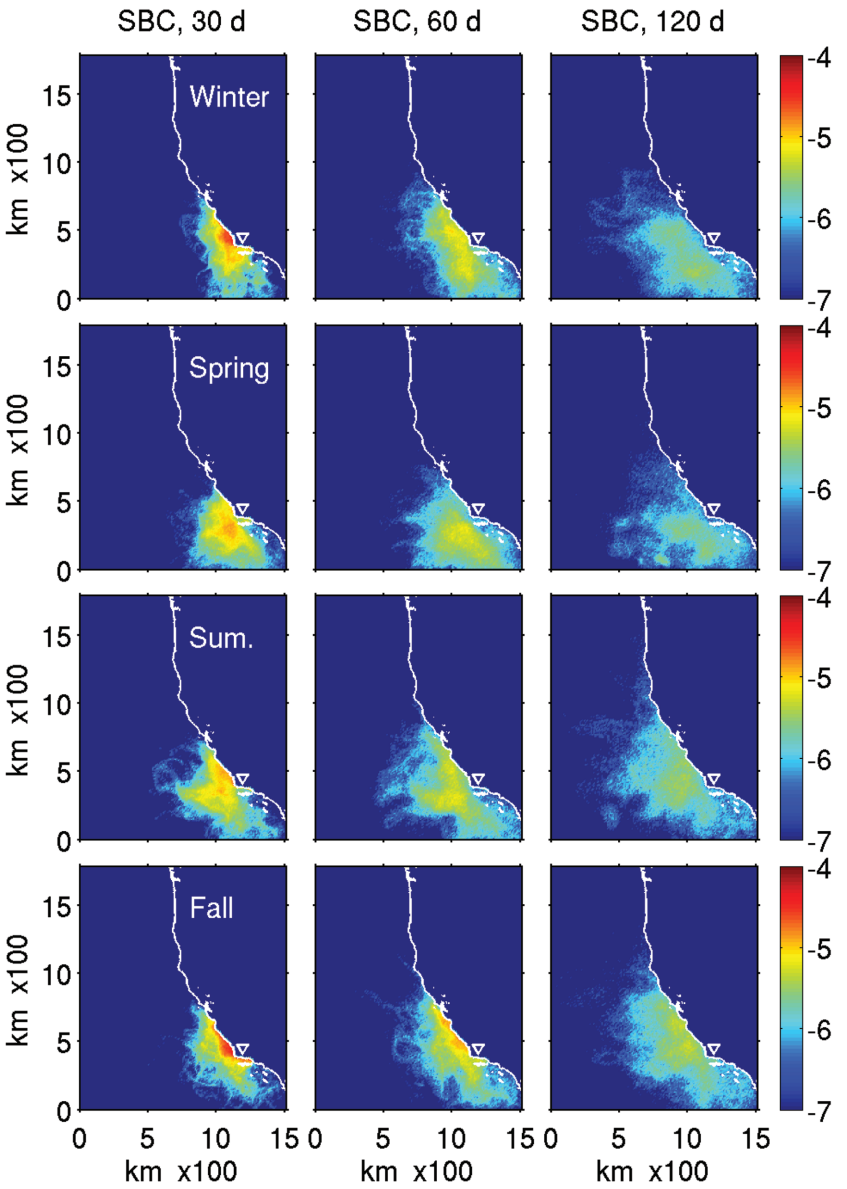

Figure 6. Climatological particle density (km^{-2}, shown with a log_{10} color scale) for the Santa Barbara Channel (SBC) release region (see Fig. 2) given a shallow (0–20 m) release for four seasons (rows) at times-since-release of 30, 60 and 120 days. Triangle indicates release location. The origin lies at (−133°E, 31°N).

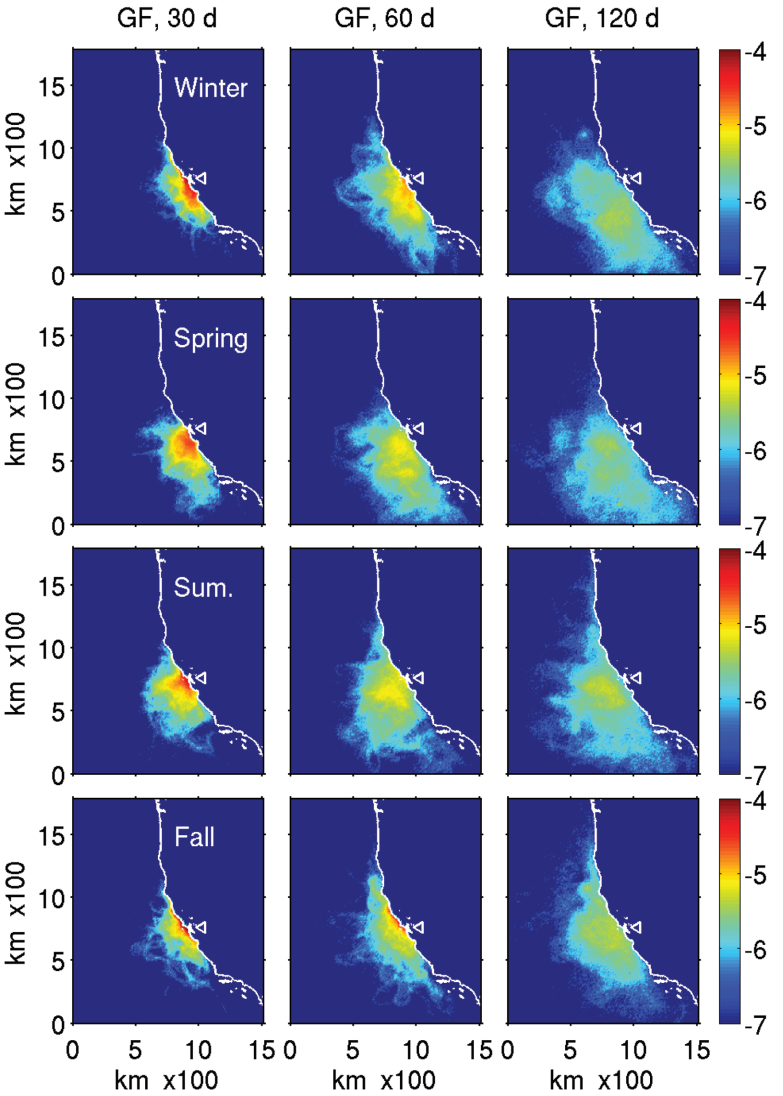

Figure 7. Climatological particle density (km^{-2}, shown with a log_{10} color scale) for the Gulf of the Farallones (GF) release region (see Fig. 2) given a shallow (0–20 m) release for four seasons (rows) at times-since-release of 30, 60 and 120 days. Triangle indicates release location. The origin lies at (−133°E, 31°N).

is broader and shifted. The modeled poleward limb is primarily confined to the shelf in spring and summer, but it transports a large percentage of floats which also diffuse away from the coast. From the SBC region, substantial numbers of particles reach the bifurcation zone at ∼5–10 days-since-release. A large fraction successfully rounds Point Conception

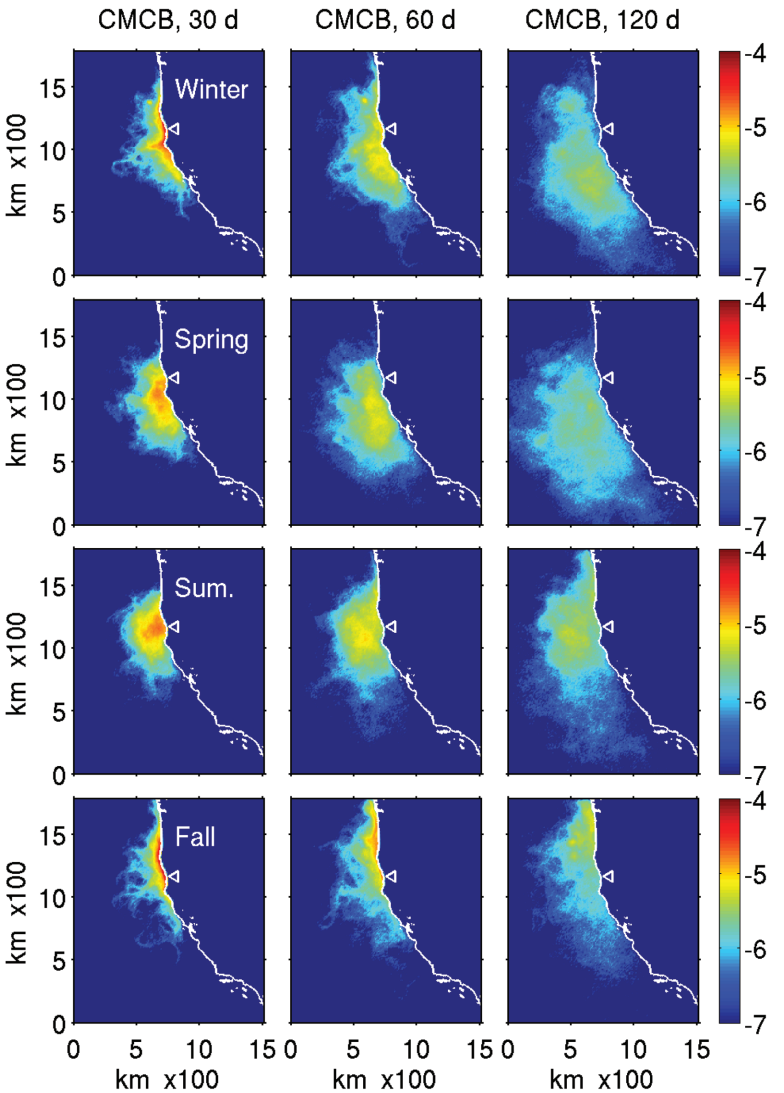

Figure 8. Climatological particle density (km^{-2}, shown with a log_{10} color scale) for the Cape Mendocino/Cape Blanco (CMCB) release region (see Fig. 2) given a shallow (0–20 m) release for four seasons (rows) at times-since-release of 30, 60 and 120 days. Triangle indicates release location. The origin lies at (−133°E, 31°N).

and moves northward, while another large fraction moves offshore southward, eventually exiting the domain. This bifurcation was found in most years. Real surface drifters in this region show this general pattern of flow, including bifurcated transport at Pt. Conception with northward transport as far as Monterey Bay (Winant *et al.,* 2003; Sotka *et al.,* 2004).

Table 2. Fraction of released floats remaining in the inner domain at various times-since-release for the full seeded coastline (FSC) and three smaller study regions (SBC, GF and CMCB, see Fig. 2) given a shallow (0–20 m) release.

	Winter	Spring	Summer	Fall
FSC at 30 d	0.98	0.99	0.99	0.90
FSC at 60 d	0.94	0.93	0.96	0.83
FSC at 120 d	0.83	0.78	0.87	0.75
SBC at 30 d	0.96	0.96	0.97	0.93
SBC at 60 d	0.84	0.74	0.85	0.90
SBC at 120 d	0.57	0.45	0.69	0.79
GF at 30 d	0.96	0.99	0.99	0.85
GF at 60 d	0.95	0.97	0.98	0.80
GF at 120 d	0.82	0.79	0.90	0.78
CMCB at 30 d	0.97	1.0	1.0	0.87
CMCB at 60 d	0.97	1.0	1.0	0.78
CMCB at 120 d	0.96	0.97	0.95	0.64

As Winant *et al.* (2003) reveal, poleward and offshore motion at the Point varies complexly with depth and time; the poleward motion is least common in springtime, consistent with our results showing fewer floats north of the point in spring than in other seasons. Surprisingly, the maximum particle densities at 60 days-since-release and later are never found in the Santa Barbara Channel (the release region) or Southern California Bight, despite the semi-enclosed nature of the release area and the recirculation in the bight.

Dispersion from the GF region (Fig. 7) is roughly symmetric in the alongshore direction for the fall release, despite strong coastal currents in the model that imply northward transport. Although these currents must influence net transport, climatological dispersion appears to be primarily diffusive for this release. In spring and summer, the transport is more southwestward, consistent with the seasonal mean velocities from the model. For all releases, most floats remain offshore of central California, between Point Conception and Cape Mendocino. Particle densities are very low in the Southern California Bight year-round, despite the large amount of net southward transport. In our model, the recirculation in the Southern California Bight does not systematically entrain a large fraction of floats from either inside or outside the bight, possibly due to its proximity to the inner domain southern boundary. The relatively few floats that do reach the bight, however, do impact connectivity as discussed below. Poleward coastal transport was greatest for the fall and summer releases, when substantial float densities are found north of Cape Blanco.

For winter and spring releases from the CMCB region (Figure 8), the majority of floats move southward, rounding Cape Mendocino. The reversal of alongshore coastal flow north of Cape Mendocino from winter to spring (Fig. 3, right panels) likely inhibits floats from

Table 3. Settlement strength (S), or the fraction of released floats that eventually settle, for the full seeded coastline (FSC) (i.e., all release cells) and three smaller study regions (SBC, GF and CMCB, see Figure 2) given a moderate (30–60 d) or long (120–180 d) PLD, 10 km settling criteria and shallow (0–20 m) release.

	Winter	Spring	Summer	Fall
FSC moderate	0.28	0.10	0.15	0.34
FSC long	0.028	0.033	0.061	0.067
SBC moderate	0.21	0.064	0.13	0.29
SBC long	0.026	0.032	0.060	0.070
GF moderate	0.36	0.10	0.18	0.43
GF long	0.025	0.036	0.051	0.063
CMCB moderate	0.35	0.088	0.10	0.37
CMCB long	0.025	0.027	0.068	0.067

progressing substantially north of Cape Blanco. For the summer case, the density at 30 days-since-release agrees well with real trajectories released off Oregon (Sotka *et al.,* 2004) during this season. The floats diffuse substantially but the cloud remains centered near the release site. The fall transport contrasts greatly with the southward motion found in winter and spring releases. In fall, floats remain relatively close to the coast and transport is primarily poleward. Most floats can be found north of Cape Blanco at 120 days-since-release.

Disabling the vertical random walk had a relatively minor effect on the overall float densities (not shown). However, slight differences near the coast did affect connectivity. Likewise, changing the release depth to 40–60 m altered overall horizontal float densities little, but did impact dispersal and connectivity. Both of these issues are explored below.

5. Settling particles

a. Settlement strength

The settlement strength (S), the fraction of floats that eventually settle along the coast, varied greatly with season, PLD and region (Table 3). For the moderate (30–60 day) PLD, a large fraction settle, with highest values for fall and winter releases. For the long (120–180 day) PLD, settlement was highest for summer and fall releases. This pattern is consistent with the seasonal upwelling cycle (Checkley and Barth, 2009). Upwelling favorable winds and their associated offshore Ekman transport are consistently highest in spring and summer (Figs. 3 and 4). These dynamics result in more southwestward particle transport away from the coast during these seasons (Fig. 7, rows 2 and 3), resulting in lower float densities at the coast and fewer opportunities for settlement. During fall and winter, wind directions are more variable and often downwelling favorable, resulting in higher densities at the coast and more opportunities for settlement. The settlement strength of the

Table 4. Mean (D_m) and standard deviation (D_{std}) of alongshore dispersal distance, in terms of arc-length of coastline (km), positive poleward, for the full seeded coastline (FSC) and smaller study regions given a moderate (30–60 d) or long (120–180 d) PLD, 10 km settling criteria and shallow (0–20 m) release.

	Winter		Spring		Summer		Fall	
	D_m	D_{std}	D_m	D_{std}	D_m	D_{std}	D_m	D_{std}
FSC moderate	31	202	−22	217	110	181	139	179
FSC long	−191	424	−118	540	211	476	202	427
SBC moderate	203	159	150	161	209	199	230	186
SBC long	45	345	116	447	394	480	317	407
GF moderate	11	160	−88	152	39	148	84	131
GF long	−238	345	−203	507	152	511	121	429
CMCB moderate	−31	193	−154	187	85	158	140	184
CMCB long	−416	448	−331	496	136	330	211	371

120–180 day PLD leads this cycle in wind forcing by one season due to longer time spent in the water column (i.e., by identification using season of release rather than settlement).

b. Dispersal distances

Table 4 gives the mean (D_m) and standard deviation (D_{std}) of alongshore dispersal distance for various regions, seasons and PLDs given a 10-km distance-from-shore settling criteria and shallow (0–20 m) release. Particles settled when they were first inside a cell during their competency window. Distance was calculated as an integrated arc-length of coastline from source to settlement locations, using the functional coastline in the model, positive poleward. Limits of integration were determined as those points on the functional coastline closest to each particle's release and settling positions. For the full seeded coastline (FSC) and moderate PLD, the mean dispersal distance is largest in summer and fall when settlement is also high (Table 3) and smallest in winter and spring. The standard deviation is greatest during these seasons, however, and an order of magnitude larger than the mean. For the full seeded coastline and long PLD, mean dispersal is equatorward in winter and spring when settlement is relatively low and is poleward in the remaining seasons. Except for summer and fall releases with moderate PLDs, the standard deviation is always greater than the absolute value of the mean by a factor of at least $\sim$2. For the FSC, PDFs of dispersal distance (not shown) were generally symmetric about the mean for both PLDs.

For the SBC region, mean distances are always poleward regardless of PLD. Except for the long PLD and winter release, the mean and standard deviation are of the same scale. Mean distances do not appear to be biased poleward by the proximity of the SBC region to the domain's southern boundary (which would prevent settlement far to the south) as

settlement was relatively low near the domain's southern edge. For the GF region, mean distances are typically small relative to the standard deviation, as with the full seeded coastline. In the GF case, D_m is strongly negative in winter and spring for the long PLD. For the CMCB region, D_m is large and negative in winter and spring given a long PLD, but always poleward in summer and fall. Except for the winter release with moderate PLD, the mean and standard deviation are typically of the same scale for this region. We note that results from the CMCB region in summer and fall may be biased low due to float loss at the northern boundary. Given a moderate PLD, PDFs of dispersal were generally symmetric about the mean for all regions (not shown). But unlike the FSC case, regional PDFs for long PLDs were often skewed and not necessarily unimodal.

6. Coastal connectivity

a. General patterns

Dispersal is the fundamental process linking many marine populations (Karlson, 2006). However as noted in the Introduction, the degree of connectedness between local populations is generally unknown. A local population may be self-sustaining, it may act as a source of individuals for distant populations that might go extinct otherwise, it may require distant recruits to sustain itself, or it may be some combination of these possibilities (Shanks *et al.,* 2003).

We quantify connectivity as the matrix $C(p, q)$ giving the fraction of particles released from coastal cell p that settle in cell q. The calculation was performed for each release season using all seven years of settlement results. Figures 9 and 10 show connectivity for winter and spring releases, respectively, given a shallow release and 10 km settling criteria for both moderate and long PLDs. Winter and spring are the primary spawning seasons for many shelf and slope species in the California Current (Shanks and Eckert, 2005). Connectivity is presented using a log_{10} scale. Release and settling cells are given on the x and y axes, respectively. Diagonal solid lines indicate cells of local settlement, with color intensity above and below this line representing northward and southward dispersal, respectively. (Note this presentation differs slightly from previous authors: Mitarai *et al.,* 2008 and 2009.) Connectivity is highly variable along the coast and clearly influenced by major geographic features. In many cases the highest settlement is distant from the source location. A general asymmetry exists between northward and southward dispersal for many release cells. Given a moderate PLD, dispersal is primarily northward between Palos Verdes and Point Reyes in both winter and spring, and it is slightly more symmetric north of the Gulf of the Farallones in winter. Given a long PLD, dispersal is primarily southward north of Point Reyes in winter and generally symmetric from source cells within the Gulf of the Farallones in spring.

In general, the overall structure of the connectivity matrices was similar between years. The exception was 2001 when very little settlement occurred between Point Conception and Point Sur from any source cell. When calculated from the seven-year mean and

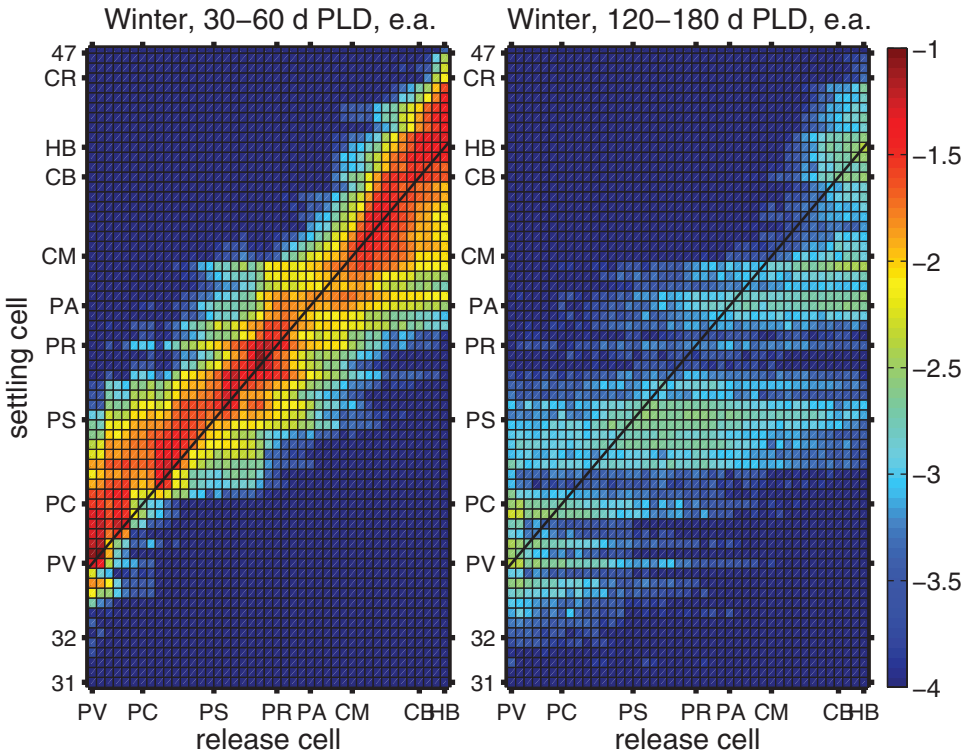

Figure 9. Winter connectivity matrices for PLDs of 30–60 d (left) and 120–180 d (right) given a 10-km settling criteria and shallow (0–20 m) release. Color indicates the fraction of particles originating from source cells on the *x*-axis that eventually settle to cells on the *y*-axis, using a log_{10} color scale. The diagonal solid line represents purely local settlement. Intensity above this line represents northward dispersal and intensity below the line, southward dispersal. PV: Palos Verdes, PC: Pt. Conception, PS: Point Sur, PR: Pt. Reyes, PA: Pt. Arena, CM: Cape Mendocino, CB: Cape Blanco, HB: Heceta Bank, CR: Columbia River mouth (see Fig. 1). Numbers on *y*-axis indicate latitudes. The horizontal bands of relatively low settlement adjacent to Point Reyes result from the protuberance of the point. Its settling cell (Figure 2, middle panel) is radially closest to more settling floats, resulting in preferential settlement.

interannual standard deviation, the coefficient of variation (c_v) represents a measure of the relative interannual variability in connectivity. Figure 11 shows this statistic with a linear color scale for a spring release and moderate PLD (left panel), and a winter release and long PLD (right panel). Values of c_v where the mean connectivity was negligible ($C(p, q) < 10^{-3.5}$) are not shown. The normalized interannual variability generally increases with distance from the source cell and is greater than one only at the fringes of settlement. For spring release with a moderate PLD, interannual variability is generally small ($c_v < 0.4$) for local settlement. For winter release with a long PLD, settlement north of Cape Mendocino is intermittent between years.

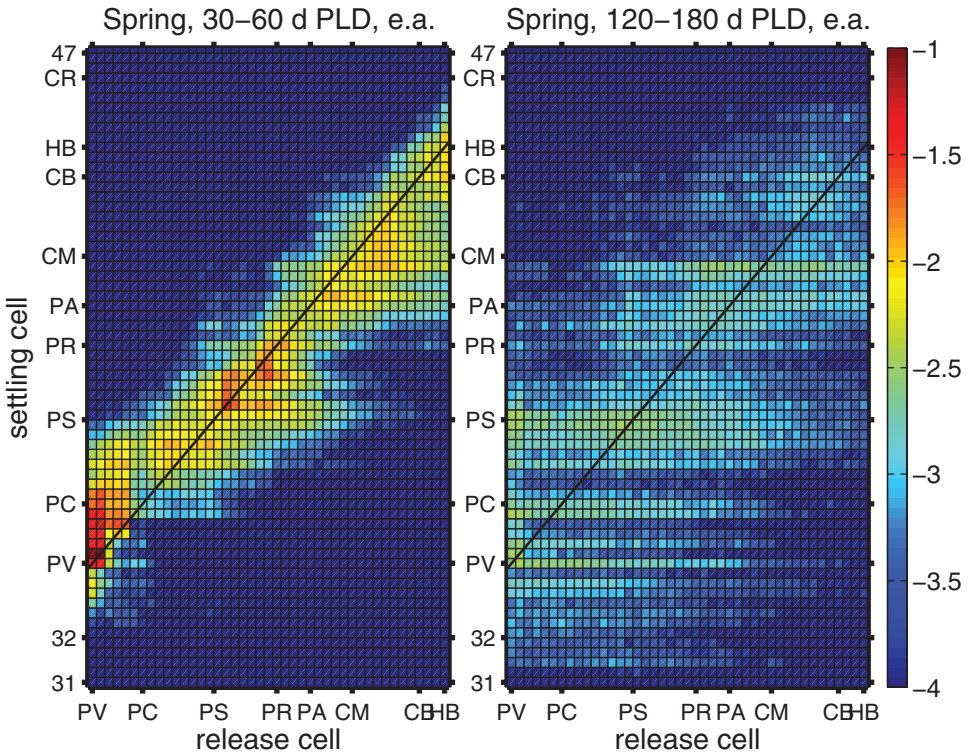

Figure 10. Spring connectivity matrices for PLDs of 30–60 d (left) and 120–180 d (right) given a 10-km settling criteria and shallow (0–20 m) release. Color indicates the fraction of particles originating from source cells on the *x*-axis that eventually settle to cells on the *y*-axis, using a log_{10} color scale. The diagonal solid line represents purely local settlement. Intensity above this line represents northward dispersal and intensity below the line, southward dispersal. PV: Palos Verdes, PC: Pt. Conception, PS: Point Sur, PR: Pt. Reyes, PA: Pt. Arena, CM: Cape Mendocino, CB: Cape Blanco, HB: Heceta Bank, CR: Columbia River mouth (see Fig. 1). Numbers on *y*-axis indicate latitudes.

b. Geographic limits

Below we outline major geographic features that coincide with dispersal limits. For a winter release and moderate PLD, the Gulf of the Farallones is the northern limit of settlement for much of the SBC region, consistent with Sotka *et al.* (2004) who show real trajectories reaching as far north as Monterey Bay and the Gulf. Likewise, Cape Mendocino defines the northern extent of settlement from the GF region. The region just north of Point Reyes is the approximate southern limit of settlement from the CMCB region, and Point Conception defines the southern limit from the GF region.

Given a winter release with a long PLD, Cape Mendocino is the approximate northern limit of settlement for most source locations from Point Sur to Point Arena. Settlement

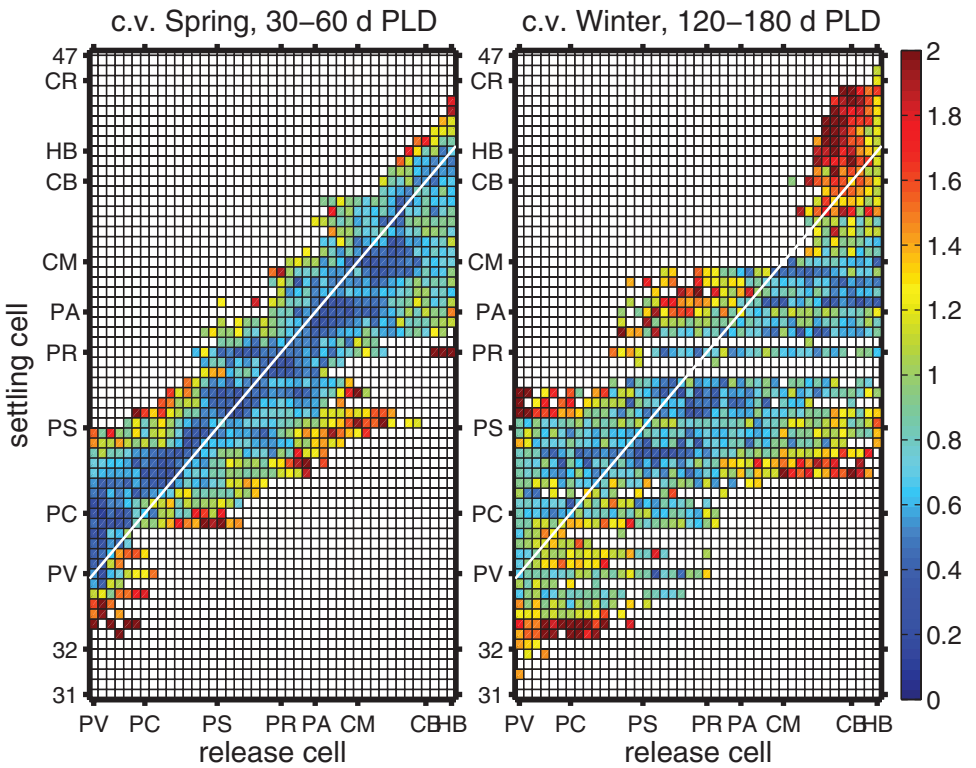

Figure 11. Inter-annual coefficient of variation (c_v) of the connectivity for a spring release and moderate PLD (left panel) and winter release and long PLD (right panel) given a 10-km settling criteria and shallow (0–20 m) release. Note a linear color scale is employed. Values where the mean connectivity was negligible ($C < 10^{-3.5}$) are not shown (white squares). c_v was calculated from the seven-year mean and the inter-annual standard deviation of the connectivity. PV: Palos Verdes, PC: Pt. Conception, PS: Point Sur, PR: Pt. Reyes, PA: Pt. Arena, CM: Cape Mendocino, CB: Cape Blanco, HB: Heceta Bank, CR: Columbia River mouth (see Fig. 1). Numbers on *y*-axis indicate latitudes.

from locations north of Cape Mendocino, including the CMCB region, extends well south of Point Sur, but does not reach Point Conception. The near-zero settlement in the Gulf of the Farallones is due to its relatively sheltered location relative to the surrounding coastline and the choice of 10 km settlement criteria with equal area for release and settlement cells.

With spring release and a moderate PLD, Point Arena is the approximate southern limit from source locations north of Cape Mendocino. Point Sur is the northern limit of settlement for many of the source locations south of Point Conception.

For a long PLD and spring release, settlement is relatively diffuse and spread over the widest geographic area of all seasons and PLDs. Settlement is locally high near the promontories of Palos Verdes, Point Conception, Point Sur and Cape Mendocino and remains low in the Gulf of the Farallones.

c. Settling criterion

Varying the spatial settlement criterion can substantially impact both settlement strength and connectivity patterns. For example, when using a 250 m isobath criterion, overall settlement strength increases by ~30–50%, relative to the 10 km distance-from-shore case described above. With the alternate criterion, each float was assigned a settling cell based on the nearest coastal point at the time during competency that it was first found inshore of the 250 m isobath. Coastal regions with wide shelves experience greater settlement than with the 10-km criterion. The 250-m isobath criterion is more appropriate for many species that settle on the outer shelf and upper slope. However, the area available for settlement assigned to each cell now varies alongshore with the shelf width, and there is not equal probability of settlement in the null case of uniformly distributed settling particles. The increase in S with the new criteria varies by release season, region and PLD, with the long PLD experiencing the greatest change. Figure 12 shows the connectivity using a 250-m criterion for both a spring release with moderate PLD (left panel) and winter release with long PLD (right panel). Given a moderate PLD, the overall pattern of connectivity is very similar to the 10-km case for all seasons (compare with Fig. 10, left panel). For the long PLD, the connectivity is again roughly similar, but important regional differences emerge. Substantially more settlement occurs in the Gulf of the Farallones with the 250-m case (compare with Fig. 9, right panel), and particles from cells south of Point Conception settle farther north to Point Arena. The horizontal bands of relatively low settlement adjacent to Point Reyes result from the protuberance of the point. Its settling cell (Fig. 2, middle panel) is radially closest to more settling floats, resulting in preferential settlement.

d. Release depth

Despite the fact that particle densities were quickly redistributed vertically after release due to the three-dimensional currents and random walk of the model, their original release depth did affect settlement and connectivity. Generally, settlement strength was ~10–100% higher given a 40–60 m release depth range (relative to the default 0–20 m case), depending on season and PLD. (Here we are using the default 10-km settling criterion). Only spring and summer releases with a moderate PLD experienced the dramatic ~100% increase. Particles released in the 40–60-m depth range initially experience onshore transport associated with coastal upwelling. As a result, their exposure to generally southeastward surface flow is delayed relative to particles with near-surface releases, leading overall to reduced dispersion and increased settlement. This effect is less significant for long PLDs because the delay associated with subsurface onshore flow represents a smaller fraction of their total pelagic period. Particles in the 40–60 m depth range also experience the upper portions of the California undercurrent or lower portions of the inshore counter-current. Mean dispersal distances were ~25–250 km more northwards for the 40–60 m case, with spring and summer releases with long PLDs experiencing a substantial ~200–250 km increase. This trend toward more northward particle transport

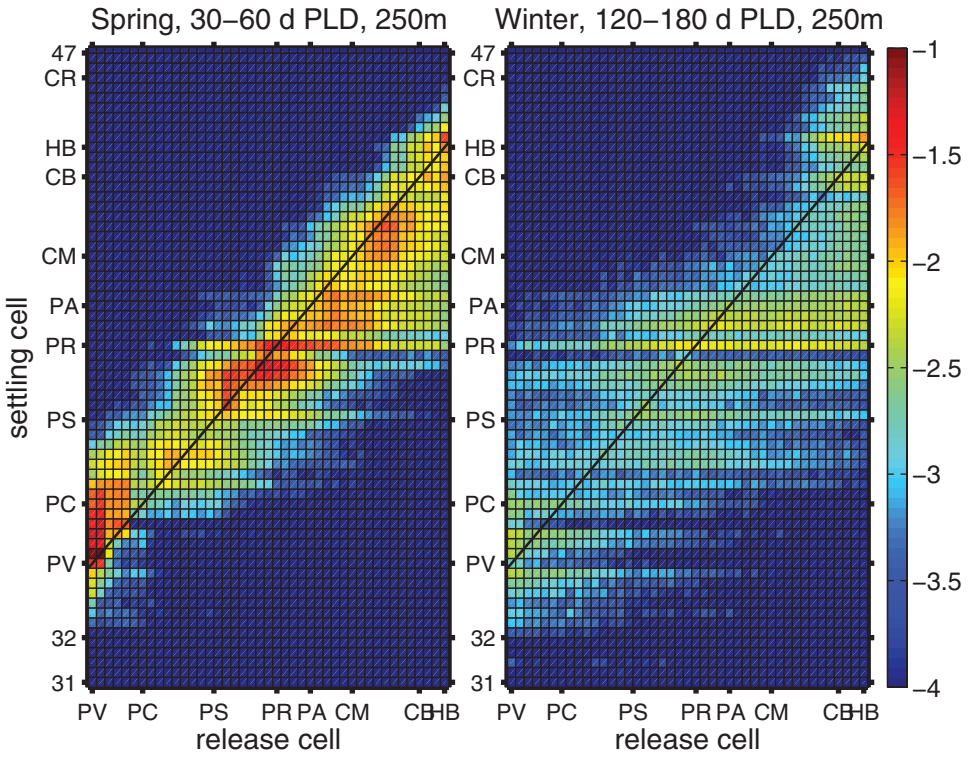

Figure 12. Connectivity matrices given a 250-m isobath settling criteria and shallow (0–20 m) release. Left panel shows a spring release with 30–60 d PLD, and the right panel shows a winter release with 120–180 d PLD. Color indicates the fraction of particles originating from source cells on the *x*-axis that eventually settle to cells on the *y*-axis, using a log_{10} color scale. The diagonal solid line represents purely local settlement. Intensity above this line represents northward dispersal and intensity below the line, southward dispersal. PV: Palos Verdes, PC: Pt. Conception, PS: Point Sur, PR: Pt. Reyes, PA: Pt. Arena, CM: Cape Mendocino, CB: Cape Blanco, HB: Heceta Bank, CR: Columbia River mouth (see Fig. 1). Numbers on *y*-axis indicate latitudes. The horizontal bands of relatively low settlement adjacent to Point Reyes result from the protuberance of the point. Its settling cell (Fig. 2, middle panel) is radially closest to more settling floats, resulting in preferential settlement.

with depth in the CCS was also discussed by Petersen *et al.* (2010). Standard deviations were comparable for both release depths. Connectivity matrices showed similar overall structure for both release depths for all seasons and PLDs, although the settlement was slightly more intense for the deeper case. Differences between depths becomes more dramatic if the vertical random walk is disabled, as can be seen in Figures 13 and 14. Figure 13 compares the connectivity of both depth ranges given a winter release and long PLD. Settlement is less patchy and more intense for the deeper case. Figure 14 shows spring connectivity given a moderate PLD. In spring, settlement is both broader and more intense for the deeper case.

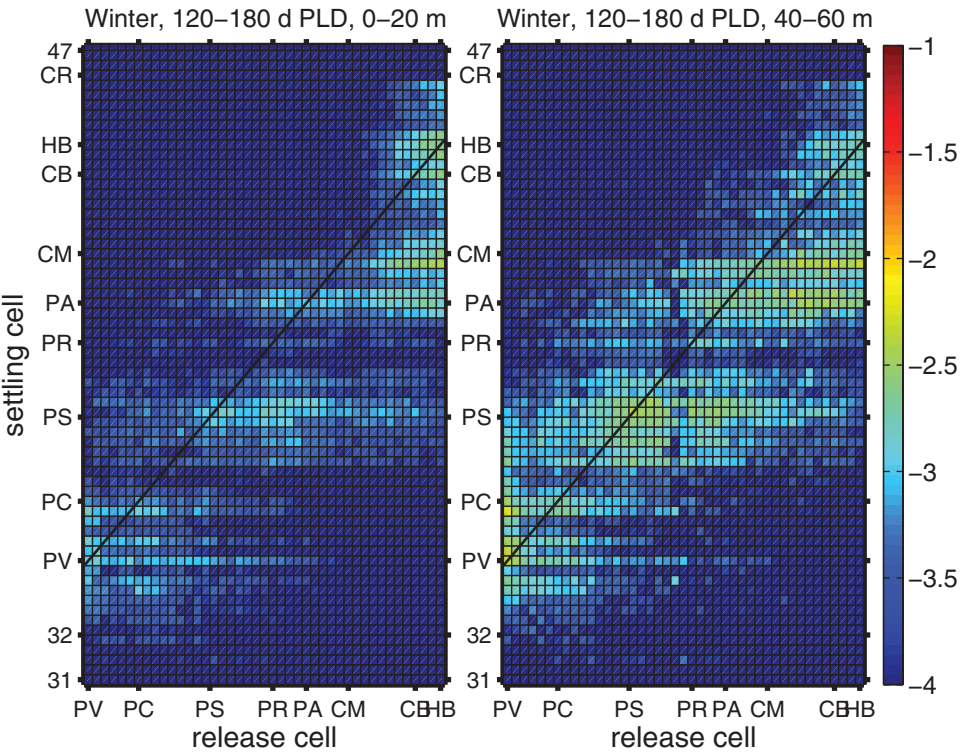

Figure 13. Winter connectivity matrices calculated without a random vertical walk given a 120–180 d PLD and 10-km settling criteria for two depths ranges. The left panel shows a shallow (0–20 m) release and the right panel shows a relatively deep (40–60 m) release. Color indicates the fraction of particles originating from source cells on the *x*-axis that eventually settle to cells on the *y*-axis, using a log_{10} color scale. The diagonal solid line represents purely local settlement. Intensity above this line represents northward dispersal and intensity below the line, southward dispersal. PV: Palos Verdes, PC: Pt. Conception, PS: Point Sur, PR: Pt. Reyes, PA: Pt. Arena, CM: Cape Mendocino, CB: Cape Blanco, HB: Heceta Bank, CR: Columbia River mouth (see Fig. 1). Numbers on *y*-axis indicate latitudes.

7. Summary and discussion

a. Summary

A realistic numerical model of the California Current System was used to study near-surface particle dispersion and coastal connectivity along the U.S. west coast. Model output compared favorably with historical surface drifter and CalCOFI data from the CCS. Modeled and measured mean near-surface currents showed similar spatial and seasonal patterns, including the seasonal appearance of an inshore counter-current. The model also captured the seasonal cycle of eddy development near the coast, and model eddy speeds were spatially correlated with drifter data in summer and fall. Climatological maps of particle density were created using seven years of modeled currents given coastal releases

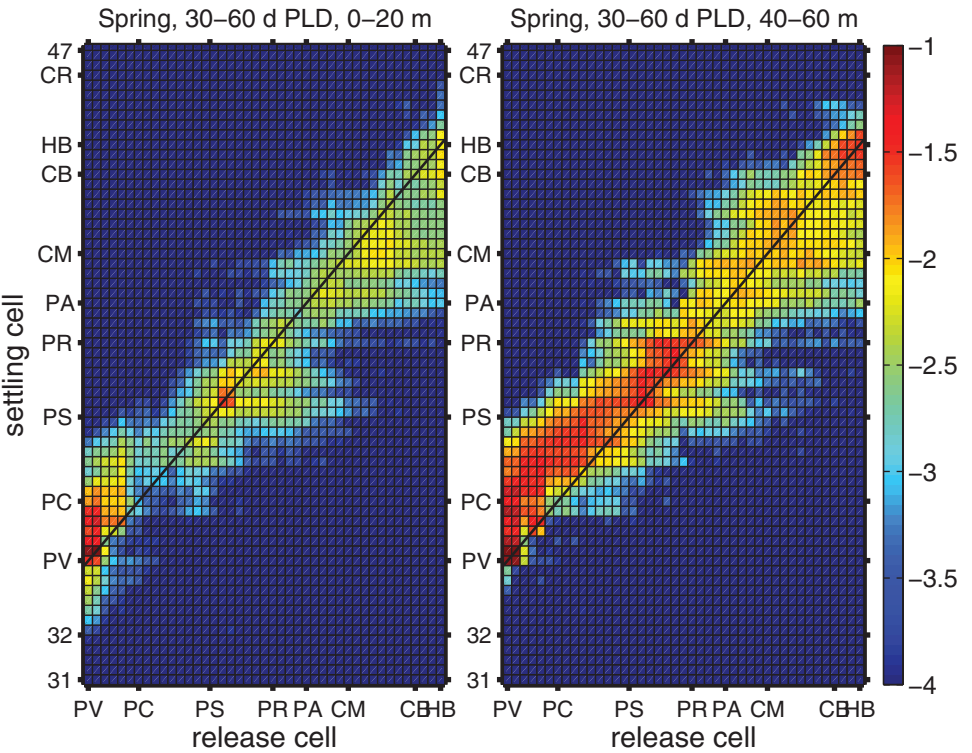

Figure 14. Spring connectivity matrices calculated without a random vertical walk given a 30–60 d PLD and 10-km settling criteria for two depth ranges. Left panel shows a shallow (0–20 m) release, and the right panel shows a relatively deep (40–60 m) release. Color indicates the fraction of particles originating from source cells on the *x*-axis that eventually settle to cells on the *y*-axis, using a log_{10} color scale. The diagonal solid line represents purely local settlement. Intensity above this line represents northward dispersal and intensity below the line, southward dispersal. PV: Palos Verdes, PC: Pt. Conception, PS: Point Sur, PR: Pt. Reyes, PA: Pt. Arena, CM: Cape Mendocino, CB: Cape Blanco, HB: Heceta Bank, CR: Columbia River mouth (see Fig. 1). Numbers on *y*-axis indicate latitudes.

of near-surface, passive particles in each of three primary zones of the CCS (southern, central and northern). Particle densities varied substantially with release season and time-since-release. At all times the majority of particles remained within the upper water column, above 60 m. Coastal connectivity showed distinct regional patterns and was clearly influenced by major headlands and embayments, and the strength and direction of dispersal varied with release location, season and depth. Given a moderate PLD, dispersal was primarily northward between Palos Verdes and Point Reyes. Given a winter release and long PLD, dispersal was primarily southward north of Point Reyes. The major headland of Point Conception did not act as a barrier to dispersal from locations to the south, but Cape Mendocino did limit northward settlement.

b. Life history traits and seasonal currents

Researchers have proposed that reproductive strategies of many species in the CCS have evolved as adaptations to the dispersal potential of ocean currents. Parrish *et al.* (1981) suggested many central California fish release their larvae in winter when upwelling is reduced and Ekman transport is minimal or primarily onshore to encourage larval retention near the coast. Others have proposed that both the timing of larval release and the length of PLD may have evolved to maximize local settlement and hence population persistence in the face of advective currents such as the predominantly southward flowing CC (Largier, 2003; Shanks and Eckert, 2005; Byers and Pringle, 2006; Shanks, 2009). In this one-dimensional view, systematic southward larval dispersal away from adult habitats could lead to eventual extinction for local populations without an adequate upstream source of larvae (Gaylord and Gaines, 2000; Gaines *et al.,* 2003). This problem is often called the "drift paradox" and was originally studied in the context of freshwater streams (Müller, 1982). Byers and Pringle (2006) suggested that many invertebrate species release larvae in April because the large-scale current fluctuations associated with the spring transition during this month (Strub *et al.,* 1987) would minimize mean dispersal distances (D_m) and maximize the diffusive spread of settling larvae (D_{std}), allowing diffusion to counteract any advective downstream transport. Shanks and Eckert (2005) propose a suite of hypotheses for fish and crustaceans that also stress the importance to persistence of minimizing D_m and maximizing D_{std}. For example, they point out that a winter release, together with a relatively long PLD (>120 d), will expose larvae to both winter and spring oceanographic regimes, wherein they will be transported first by a poleward-flowing inshore counter-current and, after the spring transition, the equatorward-flowing CC. This combination of oceanographic flows over time would allow larvae to return to their spawning habitats, despite the predominantly southward currents.

The analysis Byers and Pringle (2006) allows for a quantitative evaluation of these ideas. Using a one-dimensional population model with a Gaussian spatial structure, they derive the following requirement for local persistence of a population when there are no density-dependent effects on recruitment:

$$\ln(N_{per}) = \frac{D_m^2}{2D_{std}^2},$$

where N_{per} is the minimum number of successfully recruiting larvae (successful in the sense that they eventually reproduce) produced over an individual's lifetime needed to ensure local growth. If the larvae are passive with zero larval and post-settlement mortality, the minimum number of larvae needed for release (N_{rel}) is then: $N_{rel} = N_{per}/S$ where S is the settlement strength. The above two equations relate three important aspects of oceanic dispersal: the net movement of recruits alongshore (D_m), the alongshore diffusive scale (D_{std}), and the settlement strength (S), which is a net measure of the offshore larval loss. Given any net displacement (mean advection) in dispersal, a population will be maintained locally only if there is adequate diffusive spreading. Alternatively, S must be sufficiently

Table 5. N_{rel}, number of larvae released per individual needed to assure local population persistence given an advective current for various regions, seasons and PLDs assuming zero larval mortality, 10 km settling criteria and shallow (0–20 m) release. See Discussion for context.

Region	Winter	Spring	Summer	Fall
FSC moderate	3.6	10	8.0	4.0
FSC long	40	31	18	17
SBC moderate	11	23	13	7.2
SBC long	38	31	23	20
GF moderate	2.8	12	5.6	2.8
GF long	52	31	20	16
CMCB moderate	2.9	16	12	3.5
CMCB long	60	44	16	18

large to compensate for either strong advection or weak diffusion. Although this analysis ignores many important biological processes, such as larval behavior and mortality, it is helpful because it isolates the influence of dispersing currents.

With this framework, one can consider whether a longer PLD benefits persistence. Due to the generally red spectrum of ocean currents, a longer PLD captures more temporal variability of motion, typically increasing D_{std} (Largier, 2003) and encouraging persistence. The effect on D_m is less straightforward. The estimate of the mean current, which contributes to D_m, varies with the averaging period and may increase or decrease numerically. In our results $|D_m|$ generally increases with PLD, and D_{std} always increases (Table 4). In addition, settlement strength always decreases with PLD, discouraging persistence.

We quantify these potentially competing factors by calculating N_{rel} for various seasons, PLDs and regions (Table 5). It can be seen that long PLDs require a greater number of larvae to ensure persistence. For any release, the value is always higher for a long PLD and often an order of magnitude higher. When larval mortality is included in the analysis, the differences between PLDs are considerably more extreme. As an illustrative example, a winter release from the GF region with a 30–60 day PLD and no mortality requires 2.8 larvae to be released over an individual's lifetime to maintain a local population (Table 5). If the larvae are pelagic for a minimum of 30 days with a larval mortality rate of 0.04 d^{-1} (Ralston and Howard, 1995), at least 10 larvae would be required per individual. Similarly for a 120–180 day PLD and winter release, 52 larvae are required for persistence given zero mortality. But the number jumps to over 7,000 with a mortality rate of 0.04 d^{-1} and a minimum of 120 days in the water column. Thus our results suggest there is no evolutionary benefit to persistence inherent in the long PLDs displayed by many species when considering the larvae as purely passive drifters.

Of course, larval behavior and other complicating factors that influence dispersal would likely alter these conclusions. Swimming ability generally increases with larval develop-

ment and age (Pineda *et al.,* 2007). Winter release minimizes offshore transport relative to spring over the first 30 days in the water column (Figs. 6, 7 and 8, left panels). Developed behavior may mitigate losses during the remainder of the PLD, making a long PLD together with a winter release an optimal spawning strategy. In addition, relatively weak currents over the inner shelf (<10 km from shore) were not well-resolved by the present model, and some larvae may exploit these currents to promote retention near-shore. We have also ignored other potentially important life history traits, such as the length of the spawning season, which was held constant here at three months. As with length of PLD, organisms that spawn over longer (or shorter) periods of time will capture more (or less) temporal variability of the currents, altering D_m and D_{std} and potentially affecting persistence. Similarly, species with relatively longer reproductive life-spans will capture more interannual flow variability and will tend to have a greater D_{std}. Although these statistics and discussion are helpful in evaluating the impact of dispersal, they obviously provide no direct link back to evolutionary biology. Life history traits discussed here may be related only indirectly to large-scale currents and may primarily reflect adaptations to biological conditions, such as the feeding seasonality of adults (Moser and Boehlert, 1991) or environmental needs of the developing larvae (Strathmann *et al.,* 2002).

c. Dispersal limits and fish distributions

Modeling experiments show larval dispersal can constrain a species' geographic range by limiting recruitment spatially (Gaylord and Gaines, 2000). In our results, dispersal and coastal connectivity were clearly influenced by major geographic and bathymetric features along the coast. Many coastal species have latitudinal distributions whose limits also coincide, at least approximately, with major promontories (Hayden and Dolan, 1976; Horn and Allen, 1978), suggesting there may be limited dispersal across these features. Other species show pronounced genetic differences across headlands, such as Cape Mendocino and Point Conception, also implying limited dispersal (Gunderson and Vetter, 2006). But dispersal limits alone may not dictate species range or genetic limits. As noted by Gaylord and Gaines (2000), many spatially varying factors in addition to dispersing currents will influence species boundaries, such as temperature, substrate type, wave and turbulence exposure, the presence or absence of other important community players, and food availability. A full investigation of the problem would require the incorporation of a population model to account for many of these effects. Nonetheless, some insight can be gained from the present work.

As an example of a range limit on the U.S. west coast, the abundances of many commercially valuable species of California rockfish decline rapidly south of ~37°N near Monterey Bay and Monterey Canyon, a deep canyon which bisects the bay and shelf and extends well offshore (Williams and Ralston, 2002). Also the abundances of several other rockfish species, such as the winter-spawning bocaccio, shortbelly and chilipepper, decline abruptly north of ~40.5°N, near Cape Mendocino and its associated Mendocino Escarpment (a submarine ridge extending westward from the cape). Williams and Ralston (2002)

speculate that these coastal features may be acting as barriers to larval dispersal and therefore rockfish abundances.

Given a winter release, a long PLD and a 250 m isobath settling criterion (the appropriate parameters for the above-named species) the present study shows that settlement from most source locations between Point Conception and Point Reyes begins to decline just north of Point Arena (~39°N) and is zero north of Cape Mendocino (~40°N) (Fig. 12, right panel). Given the same release scenario, but a 10 km distance-from-shore settling criterion, Cape Mendocino becomes the distinct limit of northward dispersal for all source cells from Point Sur northward to the cape (Figure 9, right panel). As there is ample shelf habitat north of Cape Mendocino for these species (Williams and Ralston, 2002), these results support the hypothesis that ocean transport contributes to this distributional limit. The influence of ocean transport is not as clear for the decline in abundance found south of Monterey Bay. In our results, a reduction in settlement is visible near Point Sur and to the south from central California source locations for winter and spring releases and a moderate PLD (Figs. 9 and 10, left panels). With a long PLD (right panels), there is no apparent reduction in settlement along the Big Sur coast for winter and spring releases for many central California source cells. In nature, the shelf width narrows considerably along the Big Sur coast, and the reduced habitat may contribute to the observed decline. This habitat reduction is not as profound in the model due to topographic smoothing required by the 3 km resolution.

Point Conception (~34°N) has also been long known to be an important floral and faunal boundary along the U.S. west coast (Horn and Allen, 1978; Wares *et al.,* 2001; Gunderson and Vetter, 2006). In the present study, northward dispersal from the Southern California Bight to central and northern California was not impeded significantly at this major headland, regardless of season or PLD (Figs. 9 and 10). Horn and Allen (1978) find that for coastal California fishes, southern species (relative to Point Conception) are more affected by the boundary than northern species: the headland acts more as a distinct northern limit to ranges from the south than as a southern limit from the north. Gaylord and Gaines (2000) argued the persistent eddy in the Santa Barbara Channel (Dever *et al.,* 1998; Dong *et al.,* 2009) may act as a barrier to dispersal from the south, creating a northern range limit for many species near Point Conception. Using patterns of genetic diversity in barnacles, Wares *et al.* (2001) argued that the predominantly southward currents of the CCS have discouraged northward migration and gene flow around the point. In contrast, northward dispersal in our model from the SCB region occurs throughout the year, indicating that Point Conception is not a larval transport boundary from the south. This northwards dispersal is consistent with measurements that show persistent polewards flow around the point at relatively shallow subsurface depths (Winant *et al.,* 2003) and during wind relaxation events (Melton *et al.,* 2009). However, it is possible that the size of the model domain, seeding choices or fundamental model errors influenced the conclusion that Point Conception is not a boundary.

d. Model errors

In this paper, we analyzed the distributions and dispersion of passive particles released in modeled ocean currents near the U.S. west coast, ultimately yielding potential connectivity of marine populations by the circulation alone. It is important to remember the many sources of error in such a calculation. Model errors arise through discretization on a finite grid, the vertical mixing parameterization, and imperfect open boundary conditions. Topographic smoothing alters important bathymetric features, and errors in atmospheric forcing and lateral boundary conditions exist. All of these issues, particularly when combined with the nonlinear fluid dynamics, influence ocean currents, possibly significantly. We investigated sensitivities of our float results to particular modeling choices (e.g., lateral boundary conditions and vertical mixing parameterization) and found them to be small. However, results must be compared to similar calculations performed on more distinct model implementations and ultimately using data assimilative circulation estimates.

Acknowledgments. We are grateful for helpful conversations with Steve Ralston, Eric Bjorkstedt and Will White that improved this work. We also thank two anonymous reviewers for their helpful suggestions. This is contribution number 369 from PISCO, the Partnership for Interdisciplinary Studies of Coastal Oceans, a long-term ecological consortium funded primarily by the Gordon and Betty Moore Foundation and the David and Lucile Packard Foundation.

REFERENCES

Antonov, J. I., R. A. Locarnini, T. P. Boyer, A. V. Mishonov and H. E. Garcia. 2006. World Ocean Atlas 2005, Volume 2: Salinity, S. Levitus, ed., NOAA Atlas NESDIS 62, U.S. Government Printing Office, Washington, D.C., 182 pp.

Botsford, L. W., A. Hastings and S. D. Gaines. 2001. Dependence of sustainability on the configuration of marine reserves and larval dispersal distance. Ecol. Lett., *4,* 144–150.

Brink, K. H., R. C. Beardsley, P. P. Niiler, M. Abbott, A. Huyer, S. Ramp, T. Stanton and D. Stuart. 1991. Statistical Properties of the near-surface flow in the California coastal transition zone. J. Geophys. Res., *96*(C8), 14693–14706.

Brink, K. H., R. C. Beardsley, J. Paduan, R. Limeburner, M. Caruso and J. G. Sires. 2000. A view of the 1993–1994 California Current based on surface drifters, floats, and remotely sensed data. J. Geophys. Res., *105*(C4), 8575–8604.

Byers, J. E. and J. M. Pringle. 2006. Going against the flow: retention, range limits and invasions in advective environments. Mar. Ecol. Prog. Ser., *313,* 27–41.

Carr, S. D., X. J. Capet, J. C. McWilliams, J. T. Pennington and F. P. Chavez. 2008. The influence of diel vertical migration on zooplankton transport and recruitment in an upwelling region: estimates from a coupled behavioral-physical model. Fish. Oceanogr., *17,* 1–15.

Centurioni, L. R., J. C. Ohlmann and P. P. Niiler. 2008. Permanent meanders in the California Current system. J. Phys. Oceanogr., *38,* 1690–1710.

Cervantes, B. T. K. and J. S. Allen. 2006. Numerical model simulations of continental shelf flows off northern California. Deep-Sea Res. II, *53,* 2956–2984.

Checkley, D. M., Jr. and J. A. Barth. 2009. Patterns and processes in the California Current System. Prog. Oceanogr., *83,* 49–64.

Chelton, D. B., A. W. Bratkovich, R. L. Bernstein and P. M. Kosro. 1988. Poleward flow off central California during the Spring and Summer of 1981 and 1984. J. Geophys. Res., *93*(C9), 10604–10620.

Collier, M. A. and P. J. Durack. 2006. The CSIRO netCDF version of the NODC World Ocean Atlas 2005, CSIRO Marine and Atmospheric Research Paper 015.

Collins, C. A., N. Garfield, T. A. Rago, F. W. Rischmiller and E. Carter. 2000. Mean structure of the inshore countercurrent and California undercurrent off Point Sur, California. Deep-Sea Res. II, *47,* 765–782.

Davis, R. E. 1985. Drifter observations of coastal surface currents during CODE: The statistical and dynamical views. J. Geophys. Res., *90*(C3), 4756–4772.

—— 1991. Observing the general circulation with floats. Deep-Sea Res., *38,* Suppl.1, S531–S571.

Dever, E. P., M. C. Hendershott and C. D. Winant. 1998. Statistical aspects of surface drifter observations of circulation in the Santa Barbara Channel. J. Geophys. Res., *103*(C11), 24781–24797.

Dong, C., E. Y. Idica and J. C. McWilliams. 2009. Circulation and multiple-scale variability in the Southern California Bight. Prog. Oceanogr., *82,* 168–190.

Drake, P. T. and C. A. Edwards. 2009. A linear diffusivity model of near-surface, cross-shore particle dispersion from a numerical simulation of central California's coastal ocean. J. Mar. Res., *67,* 385–409.

Gaines, S. D., B. Gaylord and J. L. Largier. 2003. Avoiding current oversights in marine reserve design. Ecol. Appl., *13,* S32–S36.

Garraffo, Z. D., A. Griffa, A. J. Mariano and E. P. Chassignet. 2001. Lagrangian data in a high-resolution numerical simulation of the North Atlantic II. On the pseudo-Eulerian averaging of Lagrangian data. J. Mar. Syst., *29,* 177–200.

Gaylord, B. and S. D. Gaines. 2000. Temperature or transport? Range limits in marine species mediated solely by flow. Am. Nat., *155,* 769–789.

Gunderson, D. R. and R. D. Vetter. 2006. Temperate rocky reef fishes, *in* Marine Metapopulations, J. P. Kritzer and P. F. Sale, eds., Academic Press, San Francisco, 69–117.

Hansen, D. V. and P.-M. Poulain. 1996. Quality control and interpolation of WOCE-TOGA drifter data. J. Atmos. Ocean. Tech., *13,* 900–909.

Hayden, B. P. and R. Dolan. 1976. Coastal marine fauna and marine climates of the Americas. J. Biogeogr., *3,* 71–81.

Hodur, R. M. 1997. The Naval Research Laboratory's Coupled Ocean/Atmosphere Mesoscale Prediction System (COAMPS). Mon. Weather Rev., *135,* 1414–1430.

Hodur, R. M., J. Pullen, J. Cummings, X. Hong, J. D. Doyle, P. Martin and M. A. Rennick. 2002. The Coupled Ocean/Atmosphere Mesoscale Prediction System (COAMPS). Oceanography, *15,* 88–98.

Horn, M. H. and L. G. Allen. 1978. A distributional analysis of California coastal marine fishes. J. Biogeogr., *5,* 23–42.

Hunter, J. R., P. D. Craig and H. E. Phillips. 1993. On the use of random walk models with spatially variable diffusivity. J. Comput. Phys., *106,* 366–376.

Ivanov, L. M., C. A. Collins, P. Marchesiello and T. M. Margolina. 2009. On model validation for meso/submesoscale currents: Metrics and application to ROMS off Central California. Ocean Model., *28,* 209–225.

Ivanov, L. M., C. A. Collins, T. M. Margolina, L. I. Piterbarg and V. N. Eremeev. 2008. On westward transport processes off central California revealed by RAFOS floats. Geophys. Res. Lett., *35,* L18604, doi:10.1029/2008GL034689.

Karlson, R. H. 2006. Metapopulation dynamics and community ecology of marine systems, *in* Marine Metapopulations, J. P. Kritzer and P. F. Sale, eds., Academic Press, San Francisco, 457–489.

Kelly, K. A., R. C. Beardsley, R. Limeburner and K. H. Brink. 1998. Variability of the near-surface

eddy kinetic energy in the California Current based on altimetric, drifter, and moored current data. J. Geophys. Res., *103*(C6), 13067–13083.

Kim, S. and J. A. Barth. 2011. Connectivity and larval dispersal along the Oregon coast estimated by numerical simulations. J. Geophys. Res., *116,* C06002, doi:10.1029/2011JC006949.

Kinlan, B. P. and S. D. Gaines. 2003. Propagule dispersal in marine and terrestrial environments: A community perspective. Ecology, *84,* 2007–2020.

Largier, J. L. 2003. Considerations in estimating larval dispersal distances from oceanographic data. Ecol. Appl., *13,* S71–S89.

Locarnini, R. A., A. V. Mishonov, J. I. Antonov, T. P. Boyer and H. E. Garcia. 2006. World Ocean Atlas 2005, Volume 1: Temperature. S. Levitus, ed., NOAA Atlas NESDIS 61, U.S. Government Printing Office, Washington, D.C., 182 pp.

Lynn, R. J. and J. J. Simpson. 1987. The California Current System: The seasonal variability of its physical characteristics. J. Geophys. Res., *92*(C12), 12947–12966.

Marchesiello, P., J. C. McWilliams and A. F. Shchepetkin. 2003. Equilibrium structure and dynamics of the California Current System. J. Phys. Oceanogr., *33,* 753–783.

Melton, C., L. Washburn and C. Gotschalk. 2009. Wind relaxations and poleward flow events in a coastal upwelling system on the central California coast. J. Geophys. Res., *114* (C11016), doi:10.1029/2009JC005397.

Mitarai, S., D. A. Siegel, J. R. Watson, C. Dong and J. C. McWilliams. 2009. Quantifying connectivity in the coastal ocean with application to the Southern California Bight. J. Geophys. Res., *114,* C10026, doi:10.1029/2008JC005166.

Mitarai, S., D. A. Siegel and K. B. Winters. 2008. A numerical study of stochastic larval settlement in the California Current system. J. Mar. Syst., *69,* 295–309.

Moser, H. G. and G. W. Boehlert. 1991. Ecology of pelagic larvae and juveniles of the genus *Sebastes.* Environ. Biol. Fish., *30,* 203–224.

Müller, K. 1982. The colonization cycle of freshwater insects. Oecologia, *52,* 202–207.

Parrish, R. H., C. S. Nelson and A. Bakun. 1981. Transport mechanisms and reproductive success of fishes in the California Current. Biolog. Oceanogr., *1,*175–203.

Petersen, C. H., P. T. Drake, C. A. Edwards and S. Ralston. 2010. A numerical study of inferred rockfish (*Sebastes* spp.) larval dispersal along the central California coast. Fish. Oceanogr., *19,* 21–41.

Pfeiffer-Herbert, A. S., M. A. McManus, P. T. Raimondi, Y. Chao and F. Chai. 2007. Dispersal of barnacle larvae along the central California coast: A modeling study. Limnol. Oceanogr., *52,* 1559–1569.

Pierce, S. D., R. L. Smith, P. M. Kosro, J. A. Barth and C. D. Wilson. 2000. Continuity of the poleward undercurrent along the eastern boundary of the mid-latitude north Pacific. Deep-Sea Res. II, *47,* 811–829.

Pineda, J., J. A. Hare and S. Sponaugle. 2007. Larval transport and dispersal in the coastal ocean and consequences for population connectivity. Oceanography, *20,* 22–39.

Poulain, P.-M. and P. P. Niiler. 1989. Statistical analysis of the surface circulation in the California Current system using satellite-tracked drifters. J. Phys. Oceanogr., *19,* 1588–1603.

Ralston, S. and D. F. Howard. 1995. On the development of year-class strength and cohort variability in two northern California rockfishes. Fishery Bull. (Fish. B.—NOAA), *93,* 710–720.

Ross, O. N. and J. Sharples. 2004. Recipe for 1-D Lagrangian particle tracking models in space-varying diffusivity. Limnol. Oceanogr.—Meth., *2,* 289–302.

Shanks, A. L. 2009. Pelagic larval duration and dispersal distance revisited. Biol. Bull., *216,* 373–385.

Shanks, A. L. and G. L. Eckert. 2005. Population persistence of California Current fishes and benthic crustaceans: A marine drift paradox. Ecol. Monogr., *75,* 505–524.

Shanks, A. L., B. A. Grantham and M. H. Carr. 2003. Propagule dispersal distance and the size and spacing of marine reserves. Ecol. Appl., *13*(1), Supplement, S159–S169.

Shchepetkin, A. F. and J. C. McWilliams. 2005. The regional oceanic modeling system (ROMS): A split-explicit, free-surface, topography-following-coordinate oceanic model. Ocean Model., *9,* 347–404.

Song, Y. T. and D. B. Haidvogel. 1994. A semi-implicit ocean circulation model using a generalized topography-following coordinate system. J. Comput. Phys., *115,* 228–244.

Sotka, E. E., J. P. Wares, J. A. Barth, R. K. Grosberg and S. R. Palumbi. 2004. Strong genetic clines and geographical variation in gene flow in the rocky intertidal barnacle *Balanus glandula.* Mol. Ecol., *13,* 2143–2156.

Strathmann, R. R., T. P. Hughes, A. M. Kuris, K. C. Lindeman, S. G. Morgan, J. M. Pandolfi and R. R. Warner. 2002. Evolution of local recruitment and its consequences for marine population. Bull. Mar. Sci., 70 (Suppl.), 377–396.

Strub, P. T., J. S. Allen, A. Huyer and R. L. Smith. 1987. Large-scale structure of the spring transition in the coastal ocean off western North America. J. Geophys. Res., *92*(C2), 1527–1544.

Strub, P. T. and C. James. 2000. Altimeter-derived variability of surface velocities in the California Current System: 2. Seasonal circulation and eddy statistics. Deep-Sea Res. II, *47,* 831–870.

Swenson, M. S. and P. P. Niiler. 1996. Statistical analysis of the surface circulation of the California Current. J. Geophys. Res., *101*(C10), 22631–22645.

Umlauf, L. and H. Burchard. 2003. A generic length-scale equation for geophysical turbulence models. J. Mar. Res., *61,* 235–265.

Veneziani, M., C. A. Edwards, J. D. Doyle and D. Foley. 2009. A central California coastal ocean modeling study. Part I: The forward model and the influence of realistic versus climatological forcing. J. Geophys. Res., *114,* C04015, doi:10.1029/2008JC004774.

Wares, J. P., S. D. Gaines and C. W. Cunningham. 2001. A comparative study of asymmetric migration events across a marine biogeographic boundary. Evolution, *55,* 295–306.

Warner, J. C., C. R. Sherwood, H. G. Arango and R. P. Signell. 2005. Performance of four turbulence closure models implemented using a generic length scale method. Ocean Model., *8,* 81–113.

Warner, R. R., S. E. Swearer and J. E. Caselle. 2000. Larval accumulation and retention: Implications for the design of marine reserves and essential fish habitat. Bull. Mar. Sci., *66,* 821–830.

Williams, E. H. and S. Ralston. 2002. Distribution and co-occurrence of rockfishes (family: Sebastidae) over trawlable shelf and slope habitats of California and southern Oregon. Fishery Bull. (Fish. B.—NOAA), *100,* 836–855.

Winant, C. D., E. P. Dever and M. C. Hendershott. 2003. Characteristic patterns of shelf circulation at the boundary between central and southern California. J. Geophys. Res., 108(C2), 3021, doi:10.1029/2001JC001302.

Zhurbas, V. and I. S. Oh. 2003. Lateral diffusivity and Lagrangian scales in the Pacific Ocean as derived from drifter data. J. Geophys. Res., *108*(C5), 3141, doi:10.1029/2002JC001596.

Received: *11 August, 2010;* revised: *26 April, 2011.*